

# Massive star evolution in close binaries: conditions for homogeneous chemical evolution

H.F. Song,<sup>1,3</sup> G. Meynet<sup>2\*</sup>, A. Maeder<sup>2</sup>, S. Ekström<sup>2</sup> and P. Eggenberger<sup>2</sup>

<sup>1</sup> College of Science, Guizhou University, Guiyang, Guizhou Province, 550025, P.R. China

<sup>2</sup> Geneva Observatory, Geneva University, CH-1290 Sauverny, Switzerland

<sup>3</sup> Key Laboratory for the Structure and Evolution of Celestial Objects, Chinese Academy of Sciences, Kunming 650011

\*Corresponding author, e-mail: georges.meynet@unige.ch

Received; accepted

## ABSTRACT

**Aims.** We investigate the impact of tidal interactions, before any mass transfer, on various properties of the stellar models. We study the conditions for obtaining homogeneous evolution triggered by tidal interactions, and for avoiding any Roche lobe overflow during the Main-Sequence phase. By homogeneous evolution, we mean stars evolving with a nearly uniform chemical composition from the center to the surface.

**Methods.** We consider the case of rotating stars computed with a strong coupling mediated by an interior magnetic field. Models with initial masses between 15 and 60  $M_{\odot}$ , for metallicities between 0.002 and 0.014, with initial rotation equal to 30% and 66% the critical rotation on the ZAMS are computed for single stars and for stars in close binary systems. Close binary systems with initial orbital periods equal to 1.4, 1.6 and 1.8 days and a mass ratio equal to 3/2 are considered.

**Results.** In models without any tidal interaction (single stars and wide binaries), homogeneous evolution in solid body rotating models is obtained when two conditions are realized: the initial rotation must be high enough, the loss of angular momentum by stellar winds should be modest. This last point favors metal-poor fast rotating stars. In models with tidal interactions, homogeneous evolution is obtained when rotation imposed by synchronization is high enough (typically a time-averaged surface velocities during the Main-Sequence phase above 250 km s<sup>-1</sup>), whatever the mass losses. We give plots indicating for which masses of the primary and for which initial periods, the conditions for the homogenous evolution and for the avoidance of the Roche lobe overflow are met, this for different initial metallicities and rotations. In close binaries, mixing is stronger at higher than at lower metallicities. Homogeneous evolution is thus favored at higher metallicities. Roche lobe overflow avoidance is favored at lower metallicities due to the fact that stars with less metals remain more compact. We study also the impact of different processes for the angular momentum transport on the surface abundances and velocities in single and close binaries. In models where strong internal coupling is assumed, strong surface enrichments are always associated to high surface velocities in binary or single star models. In contrast, models computed with mild coupling may produce strong surface enrichments associated to low surface velocities. This observable difference can be used to probe different models for the transport of the angular momentum in stars. Homogeneous evolution is more easily obtained in models (with or without tidal interactions) with solid body rotation.

**Conclusions.** Close binary models may be of interest for explaining homogeneous massive stars, fast rotating Wolf-Rayet stars, and progenitors of long soft gamma ray bursts, even at high metallicities.

**Key words.** binaries:close-stars; stars: abundances; rotation;evolution

## 1. Introduction

A significant fraction of massive stars may belong to close binary systems (see e.g. Sana et al. 2012, 2013). Tidal interaction in close binary systems can change the evolution of the primary well before any mass transfer (de Mink et al. 2009a; Song et al. 2013). In particular, strong mixing can be induced leading to a nearly homogeneous evolution. Homogeneous evolution of stars is a topic of interest for many reasons: models and observations suggest the existence of such stars (Maeder 1987; Martins et al. 2009, 2013). Second, when occurring in close binary systems, such a homogeneous evolution may imply that the Roche lobe overflow will be avoided (de Mink et al. 2009a). Third, this type of evolution may be of interest as a possible scenario leading to long soft gamma-ray burst (Yoon et al. 2006). Fourth, these stars are powerful sources of ionizing photons (Meynet et al. 2008; Levesque et al. 2012; Leitherer et al. 2014) and if frequent enough in the early Universe could have contributed to its reion-

ization. Finally, such an evolution may be also of interest in the frame of the studies aiming at understanding the anticorrelations between the abundances of some light elements like oxygen and sodium observed at the surface of a large fraction of stars in globular clusters (see discussions of the observational evidences and proposed models in the reviews by Gratton et al. 2004, 2012).

Homogeneous evolution can be triggered by various mechanisms:

- 1) Very massive stars have so large convective cores that their evolution can be considered as nearly homogeneous (Maeder 1980; Yusof et al. 2013)
- 2) Strong internal mixing in radiative zones produce homogeneous evolution (Maeder 1987).

In this work, we shall focus on models with strong mixing in the radiative zones. This strong mixing can be due either to fast rotation and/or due to some Tidally Induced Shear Mixing (TISM, see more below).

Fast rotation can be the result of initial conditions, the star rotating fast on the ZAMS, or due to some accelerating mechanism induced by tidal forces, mass accretion or merging of stars.

TISM does not require any high initial rotation, it needs only the build up of strong shear gradients in the star. It will occur only in close binary systems, either when the star is spin-up or spin-down (Song et al. 2013). It can occur only in stars which have mild internal transport processes of angular momentum (like for instance transports by shear and meridional currents).

In case the transport of angular momentum is quite fast (like the one triggered by a strong internal magnetic field, as in the work of de Mink et al. 2009a, and as in most of the models computed in the present work), at every time, the star rotates nearly as a solid body and therefore the transport by the shear becomes negligible! The tidal interaction in that case mainly serves as a process to give the star a fast enough rotation to drive a homogeneous evolution. In the present work, we focus on this type of models. As such, it is a follow up of the study made by de Mink et al. (2009a), with however the following differences:

- In de Mink et al. (2009a), the space of parameters studied are massive binaries with initial masses  $20 + 15 M_{\odot}$  and  $50 + 25 M_{\odot}$ , with a composition representative of the Small Magellanic Cloud (mass fraction of heavy elements  $Z=0.0021$ ) and with initial orbital periods between 1.1 and 4 days. Here we study binaries with initial masses  $60 + 40 M_{\odot}$ ,  $50 + 33.3 M_{\odot}$ ,  $40 + 26.7 M_{\odot}$ ,  $30 + 20 M_{\odot}$ , and  $15 + 10 M_{\odot}$  for initial metallicities  $Z=0.002$ ,  $0.007$  and  $0.014$  and initial orbital periods equal to 1.4, 1.6 and 1.8 days.
- In de Mink et al. (2009a), the synchronization phase was not explicitly computed. Based on an analytical estimate of the synchronization timescale, these authors showed that this time is very short, less than 1% of the Main-Sequence lifetime for the parameters considered in their work. Therefore, they began their computation assuming that the system is synchronized, the stars having rotation rates such that their spin period is equal to the orbital period. Here we computed explicitly the synchronization phase accounting for the various transport processes. We computed models with high initial surface equatorial velocities between 360 and 420 km  $s^{-1}$  on the ZAMS (see Tables A.1 and A.2), that correspond to the cases of spin-down by the tidal forces and models with moderate initial surface equatorial velocities between 150 and 175 km  $s^{-1}$  on the ZAMS, that correspond to the cases of spin-up by the tidal forces.
- The physical ingredients of our models are different from those used in de Mink et al. (2009a) (see more in Section 2 below). Also, in the Appendix B, we explore the consequences of tidal interactions when two different transport mechanisms for the angular momentum are considered. One which produces a mild coupling between the core and the envelope mediated by only shear and meridional currents and the other one, which is a strong coupling, mediated by an internal magnetic field. As we will see the consequences of the tidal interactions are very different.

In Section 2, we discuss the physical ingredients of the models. The results for  $40 M_{\odot}$  models, single and in close binaries, are presented in Section 3. The models for stars with masses between 30 and  $60 M_{\odot}$ , with and without tidal interaction are discussed in Section 4. Section 5 discusses the conditions for obtaining a homogeneous evolution and for avoiding Roche lobe overflow in a close binary system. Section 6 synthesizes the conclusions and indicates some further works both observational and theoretical that appear interesting to be done along this line

of research. The Appendix A present tables indicating some properties of the stellar models computed in this work. The Appendix B is devoted to a discussion of the effects of tidal interactions on systems composed of a 15 and  $10 M_{\odot}$  for two different treatments of the transport of the angular momentum.

## 2. Physical ingredients of the models

Except for what concerns the effects of rotation and of the tidal forces, the present models use the same physical ingredients as in the works by Ekström et al. (2012); Georgy et al. (2013a,b). In particular, we use the Schwarzschild criterion with a moderate overshoot for computing the size of the convective core. The overshooting parameter is taken equal to 10% the pressure scale height estimated at the border of the convective core given by the Schwarzschild's criterion. Note that the models by de Mink et al. (2009a) use a much higher overshooting parameter of 35.5% the pressure scale height estimated at the border of the Ledoux's boundary, based on calibrations by Brott et al. (2011).

The impact of the tides in close binary system is accounted for as in Song et al. (2013). A significant difference however with respect to the work by Song et al. (2013) is that here we assume a strong internal coupling mediated by an internal magnetic field. More precisely we performed the computation including the equations of the Tayler-Spruit dynamo (Spruit 2002) as given in Maeder & Meynet (2005). In this framework, for the mixing of the chemical species, we use the following equations:

$$\rho \frac{dX_i}{dt} = \frac{1}{r^2} \frac{\partial}{\partial r} \left( \rho r^2 [D + D_{\text{eff}}] \frac{\partial X_i}{\partial r} \right) + \left( \frac{dX_i}{dt} \right)_{\text{nuc}}$$

with  $\rho$  the density,  $X_i$ , the mass fraction of element  $i$ ,  $t$ , the time,  $r$ , the radius,  $D$  and  $D_{\text{eff}}$ , the diffusion coefficients (see below). The last term on the right hand side expresses the changes of the mass fraction of element  $i$  resulting from nuclear reactions. In the above expression,  $D = D_{\text{shear}} + D_{\text{magn}}$  with

$$D_{\text{shear}} = f_{\text{energy}} \frac{H_P}{g\delta} \frac{K}{\left[ \frac{\varphi}{\delta} \nabla_{\mu} + (\nabla_{\text{ad}} - \nabla_{\text{rad}}) \right]} \left( \frac{9\pi}{32} \Omega \frac{d \ln \Omega}{d \ln r} \right)^2$$

where  $K = \frac{4ac}{3\kappa} \frac{T^4 \nabla_{\text{ad}}}{\rho P \delta}$ , and with  $f_{\text{energy}} = 1$ , and  $\varphi = \left( \frac{\partial \ln \rho}{\partial \ln \mu} \right)_{P,T} = 1$ . The quantity  $H_P$  is the pressure scale height,  $g$ , the gravity,  $\delta = -(\partial \ln T / \partial \ln \rho)_{\mu,P}$ ,  $\nabla_{\text{ad}}$ ,  $\nabla_{\text{rad}}$  and  $\nabla_{\mu}$  are respectively the adiabatic, radiative temperature gradients and the mean molecular weight gradient,  $\Omega$ , the angular velocity,  $T$ , the temperature,  $P$ , the pressure,  $\kappa$ , the opacity,  $a$ , the radiation constant and  $c$ , the velocity of light. We have also

$$D_{\text{eff}} = \frac{1}{30} \frac{|r U(r)|^2}{D_h}$$

with

$$D_h = \frac{1}{c_h} r |2V(r) - \alpha U(r)|$$

where  $\alpha = \frac{1}{2} \frac{d \ln(r^2 \Omega)}{d \ln r}$  and  $c_h = 1$ ,  $U(r)$  and  $V(r)$  are the radial dependence of respectively the vertical and horizontal component of the meridional circulation velocity. To define the magnetic diffusivity  $D_{\text{magn}}$ , we first have to obtain the Alfvén frequency  $\omega_A$  by solving the equation

$$\frac{r^2 \Omega}{\left( \frac{d \ln \Omega}{d \ln r} \right)^2} K \left( N_{\mu}^2 + N_T^2 \right) x^4 - \frac{r^2 \Omega^3}{K} x^3 + 2N_{\mu}^2 x - 2\Omega^2 \left( \frac{d \ln \Omega}{d \ln r} \right)^2 = 0$$

with  $x = \left(\frac{\omega_A}{\Omega}\right)^2$ ,  $N_T^2 = \frac{g\delta}{H_p}(\nabla_{\text{ad}} - \nabla_{\text{rad}})$  and  $N_\mu^2 = \frac{g\varphi}{H_p}\nabla_\mu$ .  $D_{\text{magn}}$  comes then as:

$$D_{\text{magn}} = \frac{r^2 \Omega}{\left(\frac{d \ln \Omega}{d \ln r}\right)^2} \left(\frac{\omega_A}{\Omega}\right)^6.$$

For the transport of the angular momentum, we use the following equation

$$\rho \frac{d}{dt} (r^2 \Omega)_{M_r} = \frac{1}{r^2} \frac{\partial}{\partial r} \left( \rho r^4 D \frac{\partial \Omega}{\partial r} \right)$$

with  $D = D_{\text{shear}} + D_{\text{magn},\Omega} + D_{\text{circ,H}}$ . In this expression,

$$D_{\text{circ,H}} = \left| \frac{r U(r)}{5 \frac{d \ln \Omega}{d \ln r}} \right|$$

and

$$D_{\text{magn},\Omega} = \frac{r^2 \Omega}{\left|\frac{d \ln \Omega}{d \ln r}\right|} \left(\frac{\omega_A}{\Omega}\right)^3 \frac{\Omega}{N_{\text{Vais}}}$$

with the general Brunt-Väisälä frequency

$$N_{\text{Vais}}^2 = \frac{D_{\text{magn}}}{2K} \frac{g\delta}{H_p} |\nabla_{\text{rad}} - \nabla_{\text{ad}}| + \frac{g}{H_p} \nabla_\mu.$$

We consider that the minimum shear for the dynamo to work is given by

$$\frac{d \ln \Omega}{d \ln r} > q_{\text{min}}$$

where  $q_{\text{min}} = \left(\frac{N_{\text{Vais}}}{\Omega}\right)^{(7/4)} \left(\frac{D_{\text{magn}}}{r^2 N_{\text{Vais}}}\right)^{(1/4)}$ .

As can be seen from the expression for the transport of the angular momentum, we accounted for the effect of meridional currents on the transport of the angular momentum through a diffusive equation instead of an advective one as we usually do in models without magnetic field. We can justify this way of doing by the following arguments: first, in models with magnetic field, the distribution of angular momentum inside the star is dominated by the processes linked to the magnetic field which is a diffusive one and no long by the meridional currents (which is an advective process); Second, the transport by a magnetic field is so efficient that it imposes at every instant a nearly flat distribution of the angular velocity inside the star. Actually the present models are equivalent to solid-body rotating models. Would we have accounted for the meridional currents as an advective process, this would not have changed that conclusion and we checked numerically that point. Indeed, in Maeder & Meynet (2005), we checked that nearly solid-body rotation is achieved in models where the meridional currents are treated as an advective process and where the major processes governing the transport of the angular momentum are those associated to the magnetic instabilities. We can note that keeping the advection by meridional currents for the transport of the angular momentum imposes the use of extremely short time steps and thus is very costly in CPU time. This would have made impossible the computation of the  $\sim 100$  different stellar models that we discuss in the present work.

Let us note that the dynamo theory proposed by Spruit (2002) has been criticized by Zahn et al. (2007). These last authors consider that the analytic treatment by Spruit (2002) is too simplified to be applied to the real stellar situation. On the other hand, the present models can be seen as a study of solid body rotating models, whatever the physical cause is held responsible

for the building up of this solid body rotation. Actually most of the chemical mixing is not due to the specific dynamo process but to the meridional currents expected to be present in solid body rotating stars. Let us remind here that the concomitant effects of meridional currents and of the strong horizontal turbulence allow to consider the mixing of the chemical species driven by these processes through a diffusive equation (diffusion coefficient  $D_{\text{eff}}$ ). Thus for the chemical mixing, in contrast to angular momentum, a diffusive treatment is anyway the one that has to be applied.

Computations of the models indicated in Sect. 1 were performed until the primary fills in its Roche lobe. In case, the primary does not succeed to fill in its Roche lobe, the computation was performed until the end of the Main-Sequence phase. For purpose of comparison, computations of single star evolution have been performed for initial masses equal to the mass of the primaries and for the same initial rotational velocities as the one considered in the close binary systems.

As we shall see in the following, some of our models may enter a phase during which the mass fraction of hydrogen at the surface becomes lower than 0.3 and the effective temperature is larger than 4.0. In that case, we consider our model star to be a  $\text{WR}_e$ , *i.e.* as a Wolf-Rayet star defined from stellar evolution criteria. The  $\text{WR}_e$  may not be exactly equivalent to the bona fide WR stars classified according to spectroscopic criteria (see for instance the discussion in Groh et al. 2014), however there is some good overlap between these two definitions.

We have calculated grids of single and binary stars in the range of masses 30 to 60  $M_\odot$ , with mass ratios equal to 3/2. We have considered 3 metallicities  $Z=0.014, 0.007, 0.002$  to cover objects in the solar neighborhood, the LMC and SMC. A variety of orbital periods and of initial axial rotation velocities is considered, so that on the whole the evolutions of 96 different systems are calculated.

### 3. The 40 $M_\odot$ stellar models

Before to present a global overview of all the results, let us first discuss the specific cases of 40  $M_\odot$  models.

In Figs. 1 and 2, the evolutions of the surface equatorial velocities (left panel) and of the tracks in the theoretical HR diagram are shown (right panel) for both single and close binary 40  $M_\odot$  stellar models (orbital period is 1.4 days). In Fig. 1, in binary systems, the primary star begins with an angular velocity larger than the orbital one and thus we have a spin-down case, while in Fig. 2, we have a spin-up case.

Let us first discuss the single star models. The most striking effect to be noted is that at the metallicity  $Z=0.014$ , the surface velocities strongly decrease as a function of time as a result of the angular momentum losses driven by the stellar winds. This occurs for initially fast and moderately rotating models. The contrast with the angular velocity at the center and the angular velocity at the surface is quite small illustrating the strong coupling induced by the magnetic field. The core begins to rotate significantly faster than the envelope only at the very end of the Main-Sequence. This comes from the ever increasing inhibiting effect of the  $\mu$ -gradient at the border of the convective core when evolution goes on. The  $\mu$ -gradients decrease the transport by magnetic fields and therefore the strong coupling. The contrast is stronger in models with  $Z=0.014$  than in the model at  $Z=0.002$ . This comes from the fact that once the coupling between the core and the envelope is no longer achieved, the stronger mass loss rates at higher metallicities increase faster the contrast between the central and the surface rotation rate.

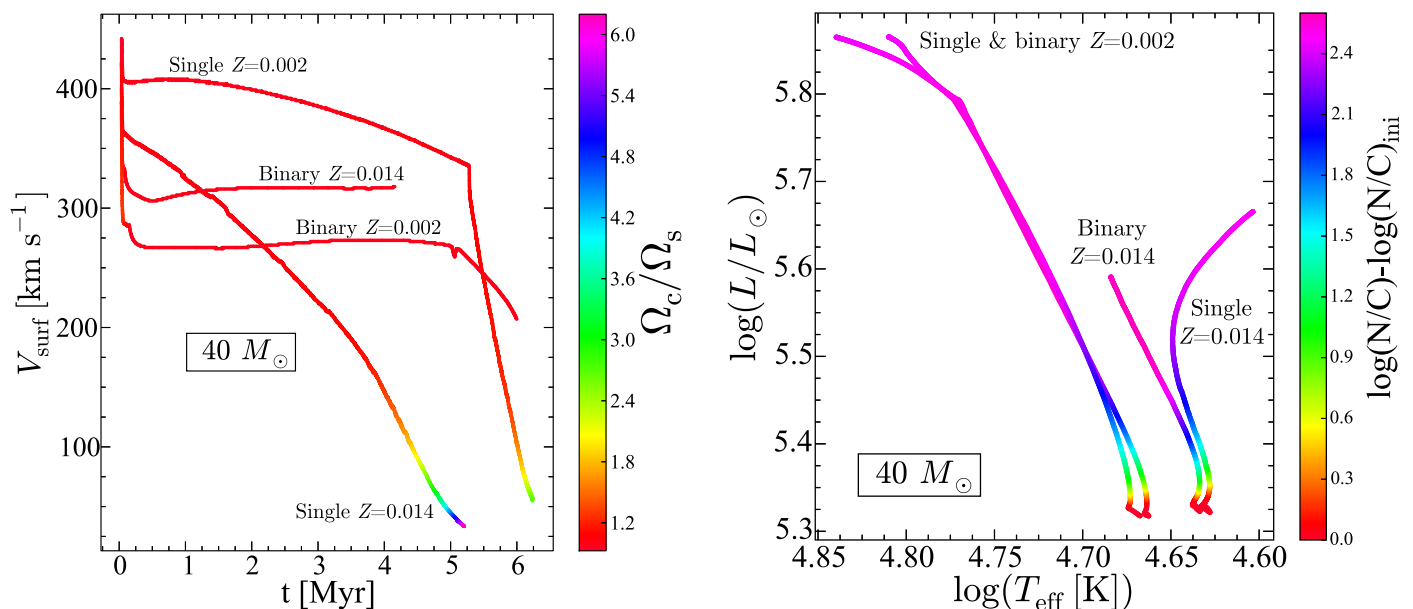


**Fig. 1.** *Left panel:* Evolution of the surface equatorial velocity as a function of time for  $40 M_\odot$  models. The colors indicate the ratio between the central angular velocity and the surface one. The orbital period for the binary models is 1.4 days, the secondary has an initial mass equal to  $26.7 M_\odot$ . *Right panel:* Evolutionary tracks in the HRD for the same models as in the left panel. The colors indicate the N/C ratio at the surface normalized to the initial one. In the binary systems, the stars have initially an angular velocity superior to the orbital one and thus the tidal forces will spin-down the star (see Table A.2).

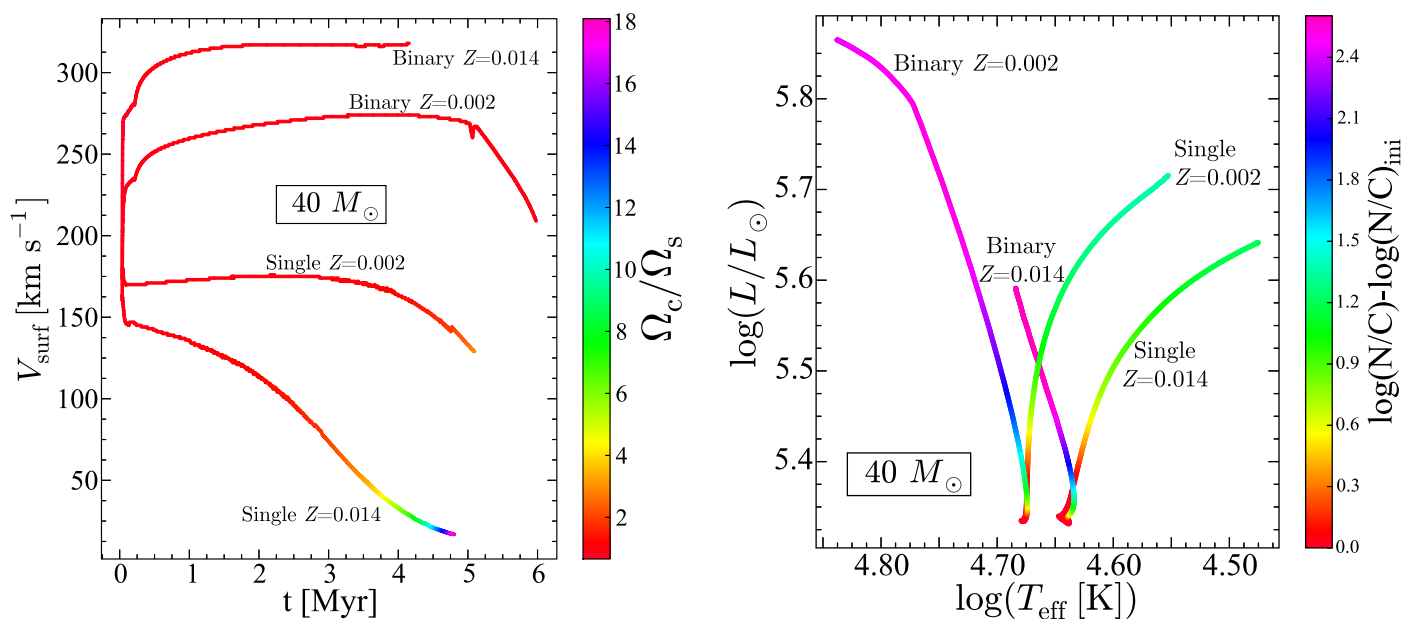


**Fig. 2.** Same as Fig. 1 for stars starting with a lower initial rotation (see Table A.2). In binary systems, the primary will be spun-up by the tidal forces.

Looking at the tracks in the HR diagram, we see that the fast rotating model at high metallicity first begins to follow the typical blueward evolution characterizing a model evolving homogeneously. Then, due to the spin down by the stellar winds, the track bends to the red. The starting point of the model with  $Z = 0.002$  is shifted to the blue because the star is more compact. This is mainly an opacity effect (see e.g. the discussion in Mowlavi et al. 1998). We see that since that model loses much less angular momentum, the mixing driven by rotation remains quite high and the star follows a nearly homogeneous evolution.

In case of models starting with a lower initial rotation (see Fig. 2), we have for the evolution of the surface velocities qual-

itatively similar behaviors as those obtained for initially fast rotating stars, the level of the surface rotation for single stars being simply shifted to lower values. This is the reason why for both metallicities considered in these plots, the evolutionary tracks for single stars evolve to the red part of the HRD as is normal for stars undergoing no or weak mixing in the radiative envelope.

Let us now discuss the close binary models. One of the main impact of the tidal interactions is to change the evolution of the surface rotation rates as can be seen in Figs. 1 and 2. We see that the changes of the surface rotation due to tidal forces is very rapid both in case of spin-down (Fig. 1) and in case of spin-up (Fig. 2).

Once synchronization is achieved, the surface velocities keep a more or less constant value for a significant part of the track (see Figs. 1 and 2). This is of course a consequence of the fact that the surface angular velocity is locked by the tidal interaction in a small domain around the orbital angular momentum velocity. We see also that since the orbital angular velocity considered is the same for the case of spin-up and spin-down, the surface velocities obtained after synchronization are very similar.

The models of  $40 M_{\odot}$  with tidal interactions are more mixed than models without tidal interactions, both in case of spin-down and in case of spin-up for the orbital periods considered here. It is of course quite natural to expect that the spin-up model is more mixed than the single star. It is a little less obvious in the case of spin-down. We can see that at  $Z = 0.014$  the spin down model has a surface rotation velocity which is larger than the single star model. This results from the fact that the single star model loses much more angular momentum than the model in the close binary. The single star loses angular momentum by stellar winds. The star in the close binary also loses angular momentum by stellar winds, but the tidal interactions compensate for these losses in order to achieve synchronization. This acceleration occurring in close binary is done through a transfer of angular momentum from the orbital reservoir to the star reservoir. Note that the amount of angular momentum in stars is very small with respect to the orbital angular momentum, so that this transfer hardly changes the orbital period and the distance between the components. So for the conditions considered here, the spin-down model in a close binary system will be more mixed than the single star mass-losing model.

At  $Z = 0.002$ , the surface velocity of the spin-down model is most of the time below the surface velocity of the single star. So here we should expect less mixing in the spin down close binary model. However this model follows a homogeneous evolution as the faster rotating model with no tidal interaction. What happens here is that both models (with and without tidal interaction) keep sufficient angular momentum to be homogeneously mixed.

In Fig. 3, the evolution of the mass fraction of hydrogen at the surface of the  $40 M_{\odot}$  stellar models are presented for the metallicities  $Z=0.014$  and  $0.002$ . The single star models starting with a larger initial rotation rate (see black and green curves in the left panel) show stronger depletion of hydrogen at the surface than those starting with a lower initial rotation (see black and green curves in the right panel). We see in particular that the single star model at  $Z=0.002$  starting with an initial rotation of  $391 \text{ km s}^{-1}$  enter into the regime when the hydrogen mass fraction at the surface become inferior to  $0.3$ . The star becomes a  $WR_e$ -type star (see Sect. 2).

The tracks of the close binary models are quite similar for the case of spin-down and spin-up, which is expected since these two models reach very rapidly the same velocities at the surface. We just note that the  $Z=0.014$  model stops at an earlier phase than the model at  $Z=0.002$  since it encounters the Roche limit while the lower metallicity models avoids it. This can be seen in Fig. 4, where the evolution as a function of time of the radii of the  $40 M_{\odot}$  models are shown. The  $Z=0.014$  close binary model crosses the Roche limit at an age equal to  $1.2 \text{ Myr}$  (both in case of spin-down and spin-up), while due to strong mixing, the  $Z=0.002$  models never crosses it during the whole MS phase.

#### 4. The whole grid of stellar models

To discuss the impact of the synchronization process on our stellar models, we introduce below a few specific times:

- $t_{\text{sync}}$ , the synchronization timescale, defined here as the time for the surface angular velocity to approach the orbital angular velocity to less than 10%;
- $t_{N/C}$ , the age of the star when, for the first time the ratio of nitrogen to carbon at the surface becomes larger than three times the initial ratio (the initial ratio is equal to 0.29 in mass fraction);
- $t_{\text{hom}}$ , the age of the star when the difference between the surface and central hydrogen mass fraction becomes larger than 10% the central hydrogen mass fraction. Even in classical (non-rotating) models, with no extra mixing, there is always a small period during which the mass fraction of hydrogen at the surface is equal or near to the mass fraction at the center since stars on the ZAMS are homogeneous and it takes some time for the central hydrogen to be depleted by more than 10%. Of course when mixing is active, this time is increased. *To some extent* this time indicates the duration of the homogeneously evolving part of the stellar lifetime (indicated by the blue shaded regions in Figs 5 and 6). We say *to some extent*, because the evolutionary track in the HR diagram can present the characteristics of a homogeneous evolution even when the difference between the surface and central hydrogen mass fraction is larger than 10%, since homogeneous evolution depends also on the way hydrogen is distributed *inside* the model and not only on the difference between the mass fraction of hydrogen at the surface and at the center.
- $t_{\text{WR}}$  is the age of the star when it enters the Wolf-Rayet (WR) phase (see Section 2).
- $t(\text{end})$  is the age of the last computed model. This age corresponds approximately to the evolutionary stage when the primary fills its Roche Volume (when this occurs) or to the end of the Main-Sequence phase (when the filling of the Roche volume does not occur).

Figures 5 and 6 show how the various times change as a function of the initial metallicity for different initial masses, rotations and orbital periods (for binary systems)<sup>1</sup>. The synchronization timescale is not shown since it is too short (shorter than  $t_{N/C}$ ). These figures allow to see the impact of the tidal forces for various initial masses, rotations and metallicities, by comparing the upper panels corresponding to single star evolution and the lower panels showing the situation when a companion is present. For each initial mass, the figures on the left column show the cases of spin-down, while the figures on the right column show the cases of spin-up.

##### 4.1. Models of single stars

Before to discuss the effects of the tidal interactions, let us discuss the results obtained for single star models or for stars in wide binary systems. In our previous works on rotating models, we showed that rotating models computed with no magnetic field present the following behavior for what concerns the efficiency of the rotational mixing: this efficiency increases with the initial mass, the initial rotation and decreases with the initial metallicity (see e.g. the discussions in Maeder & Meynet 2001; Ekström et al. 2012; Georgy et al. 2013a). From previous work, we know that models with an internal magnetic field are more mixed (Maeder & Meynet 2005), but we have never investigated how mixing triggered by magnetic instabilities behaves when the initial mass, rotation or metallicity vary. *Actually, it*

<sup>1</sup> The reader will find in the Appendix A of this paper, tables with various properties of all the models computed here, among them the precise values of the times defined just above.

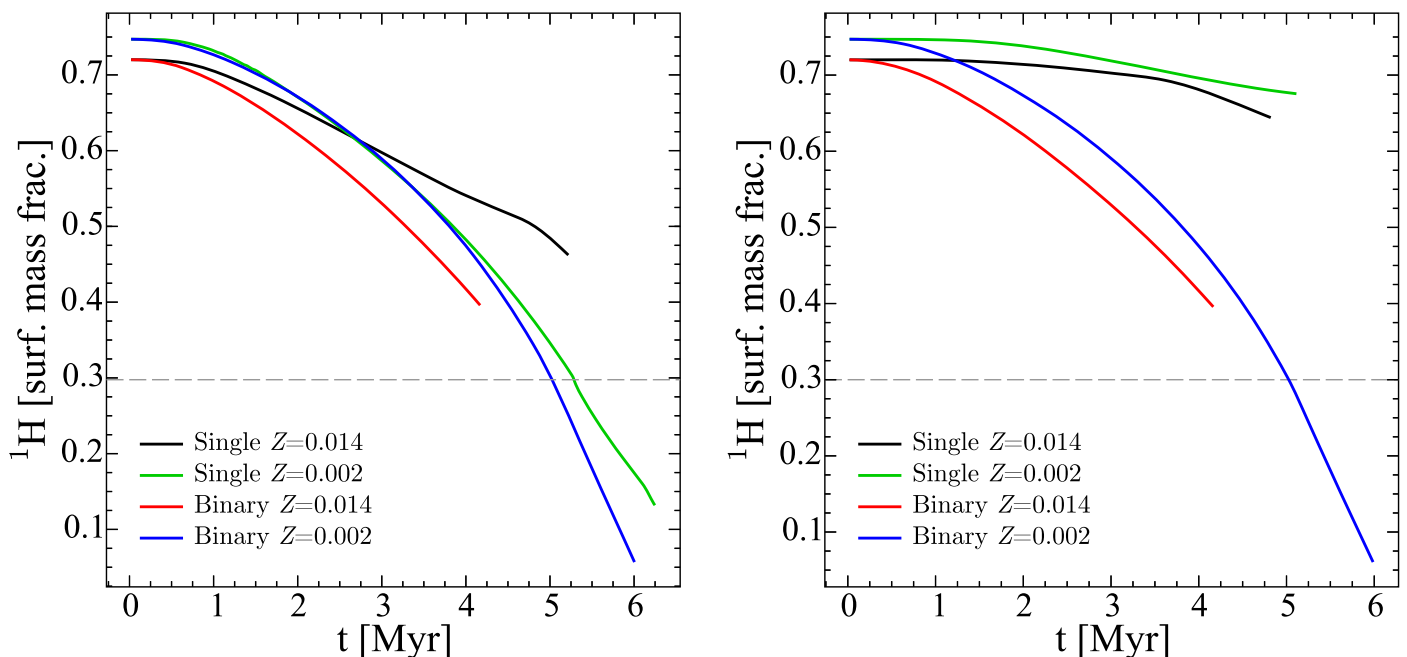


**Fig. 3.** Evolution of the surface hydrogen abundance (in mass fraction) for  $40 M_{\odot}$  models. The limit for becoming a WR star ( $X_s < 0.3$ ) is indicated with a grey dotted line. The models plotted are the same as those presented in Figs. 1 and 2. *Left panel:* Cases of spin-down. The  $Z=0.014$  and  $Z=0.002$  models have initial rotation on the ZAMS equal to respectively  $365 \text{ km s}^{-1}$  and  $391\text{-}394 \text{ km s}^{-1}$  (see Table. 1)). *Right panel:* Cases of spin-up. The  $Z=0.014$  and  $Z=0.002$  models have initial rotation on the ZAMS equal to respectively  $151 \text{ km s}^{-1}$  and  $163\text{-}167 \text{ km s}^{-1}$ .

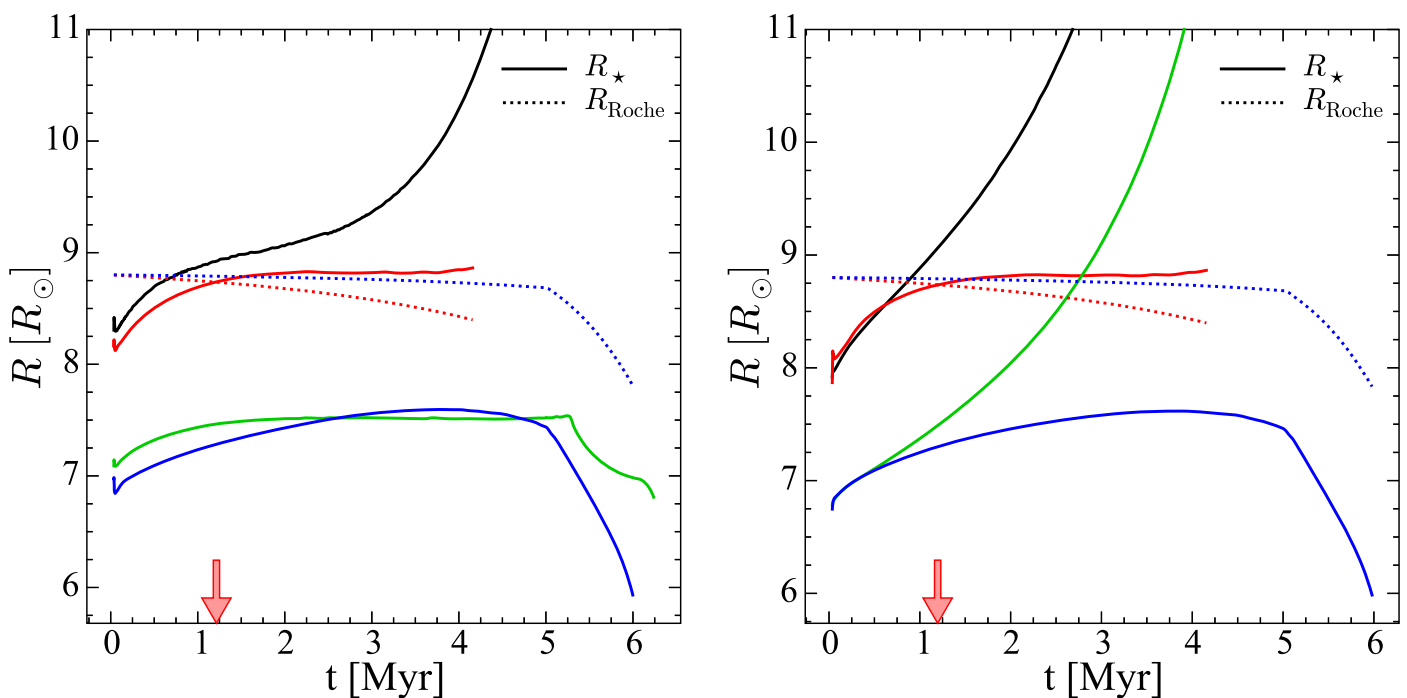


**Fig. 4.** Evolution of the stellar radius and the Roche radius for the same models as in Fig. 3 (same color code). The time at which the Roche radius is reached by the  $Z=0.014$  binary is marked with a red arrow.

*happens that these dependencies are exactly the same (qualitatively) than those that were deduced from rotating non-magnetic models.* Let us see why in the following.

Mixing in magnetic models is more efficient in higher mass stars. Comparing for instance the positions of the triangles in the upper panels of Fig. 6 corresponding to an initial rotation equal to about 30% the critical angular velocity for a  $40$  and  $30 M_{\odot}$  model (the second and the fourth panel starting from left), we see that the stage at which the N/C ratio at the surface becomes

superior to three times the initial one corresponds to about half the main sequence lifetime in the case of the  $30 M_{\odot}$  at  $Z=0.014$ , while it corresponds to about one third of the MS lifetime for the corresponding model with an initial mass equal to  $40 M_{\odot}$ . This dependence on the initial mass is such because  $U$ , the amplitude of the radial component of the meridional velocity, which is the main driving parameter for the chemical mixing in magnetic models, scales with the luminosity to mass ratio (see Eq. 11.75

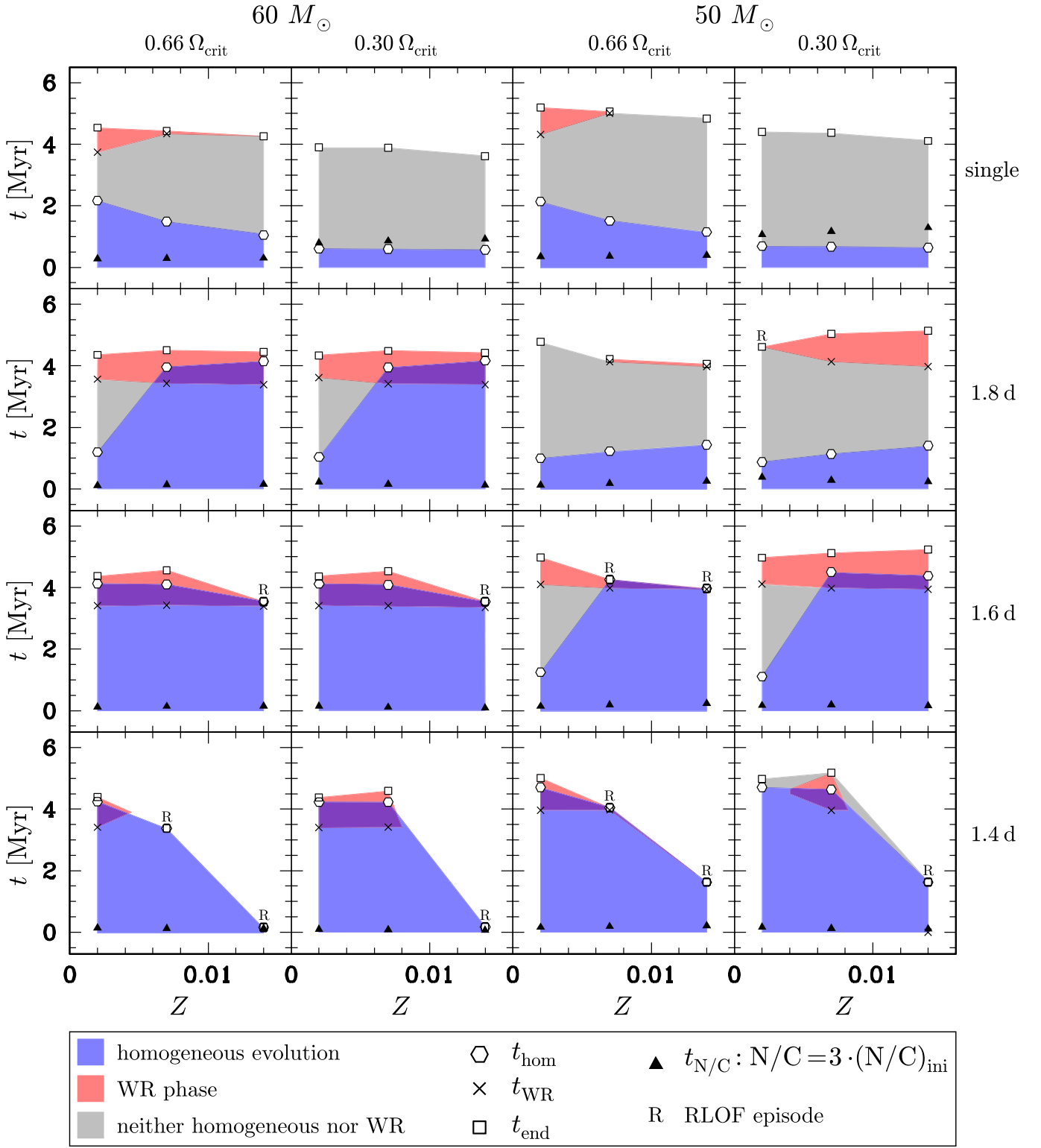


**Fig. 5.** For each stellar model, with initial masses equal to  $60$  and  $50 M_{\odot}$ ,  $t_{N/C}$  (black triangles),  $t_{\text{hom}}$  (empty hexagons),  $t_{\text{WR}}$  (crosses) and  $t_{\text{end}}$  (empty squares), the age of the last computed model (empty squares), are indicated as a function of metallicity. These times are defined in the text in Sect. 3. The blue area corresponds to the part of the evolution which is homogeneous, the red region to the WR phase. When the stellar models are neither homogeneous, nor a WR star, the region is in grey. When a R is indicated, it means that the model reaches a stage where Roche lobe overflow occurs.

in Maeder 2009), a ratio which increases when the initial mass increases.

As expected, mixing is more efficient in faster rotating models. Typically compare the positions of the triangles in Fig. 6 in the upper two right panels corresponding to single  $30 M_{\odot}$  mod-

els. We see that when the initial rotation increases, triangles are shifted to smaller times indicating that in faster rotating models, mixing is more efficient. This comes from the fact that  $U$  scales with  $\Omega$ .

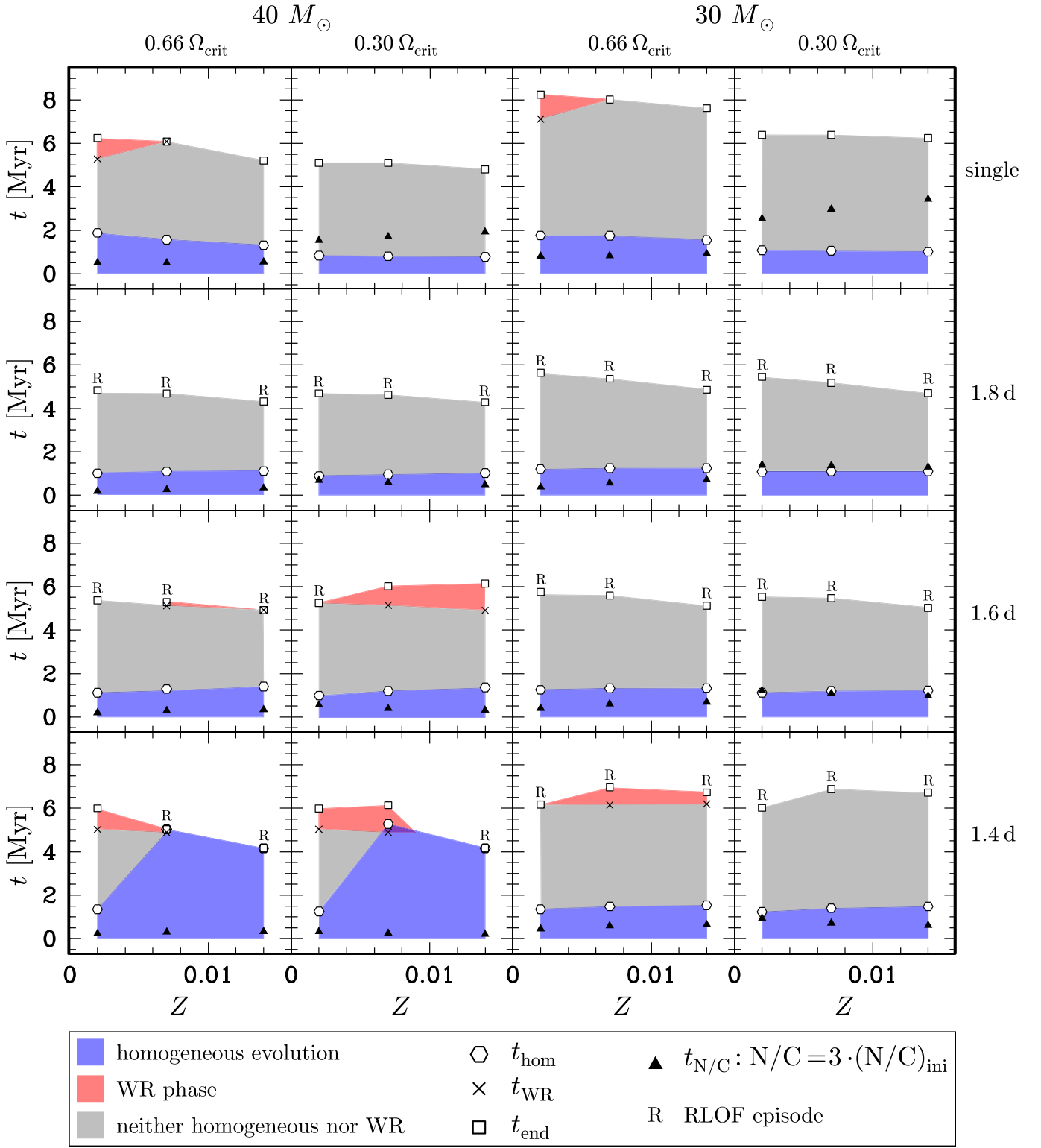


**Fig. 6.** Same as Fig. 5 for initial masses equal to 40 and 30  $M_{\odot}$ .

At higher metallicities, the stellar models are less efficiently mixed. Again this can be observed by looking at the triangle positions for instance in the upper right panel of Fig. 6. We see that for the spin-up 30  $M_{\odot}$  stellar model, the time at which  $N/C$  at the surface becomes larger than three times the initial ratio is shifted towards larger ages when higher metallicities are considered. This comes mainly from the fact that, at high metallicities, stars are efficiently slowed down by the loss of angular

momentum by stellar winds and thus are less mixed. In models with no strong stellar winds, two counteracting effects intervene that may, depending on the circumstances, trigger more or less mixing at high than at low metallicity. A rough estimate of the timescale for the mixing in the radiative zone can be obtained by the ratio of  $U$  to the radius of the star  $R$  (see Eq. 11.63 in Maeder 2009). On one hand, at higher metallicities,  $U$  is larger in the outer layers (since  $U$  scales as the inverse of the density in



this region and stars, in metal-rich regions, are larger and hence less dense in their outer layers than stars in metal-poor regions). On the other hand,  $R$  is larger at high metallicity. So the ratio  $U/R$  may increase/decrease with the metallicity. In the present paper, for the mass range considered, the effect of the mass loss dominates making the mixing more efficient in low metallicity stars.

All the single star evolutionary tracks are shown in Fig. 7 (look at the black lines). For all the initial masses considered, the faster rotating tracks at  $Z=0.002$  have a homogeneous evolution. When the metallicity increases, the fast rotating tracks (look at the upper panels for each mass) begin to bend redwards at still earlier stages. The single star tracks computed for a moderate initial rotation (lower panels for each mass) show all a classical redwards evolution during the MS phase. When the metallicity increases, the tracks are redder and less luminous.

#### 4.2. Models of close binary stars.

We can note three types of main differences between the models with and without tidal interactions: changes in the surface velocities and compositions, changes in the evolutionary tracks and possible occurrence of Roche lobe overflow event in close binary systems.

##### 4.2.1. Synchronization times

How does the synchronization time varies with the initial mass, metallicity, rotation and orbital period? For the models shown in Tables A.1 and A.2,  $t_{\text{sync}}$  is always inferior to 0.8 Myr. In general it is much shorter than this upper value and corresponds to a few percents of the MS-lifetimes.

It increases with the difference between the initial  $\Omega$  and the orbital period: see for instance the  $30 M_{\odot}$  at  $Z=0.014$  starting with an initial equatorial rotation velocity of  $365 \text{ km s}^{-1}$ , the synchronization time is 0.18 Myr when  $\Omega/\omega_{\text{orb}}=1.4$ , and equal to 0.43 Myr when  $\Omega/\omega_{\text{orb}}=1.8$  ( $\Omega$  is the stellar surface angular velocity and  $\omega_{\text{orb}}$  is the orbital angular velocity).

The dependency on the initial metallicity does appear quite weak. For instance the model B1.6 for the  $30 M_{\odot}$  model that has an initial value of  $\Omega/\omega_{\text{orb}}=1.773$  at  $Z=0.007$ , has a value of  $t_{\text{sync}}=0.36$  Myr. The model B1.4 for the  $30 M_{\odot}$  model that has an initial value of  $\Omega/\omega_{\text{orb}}=1.772$  at  $Z=0.002$ , has a value of  $t_{\text{sync}}=0.34$  Myr, so not significantly different.

The synchronization timescale decreases when larger initial masses are considered: compare for instance  $t_{\text{sync}}$  for the  $30 M_{\odot}$  at  $Z = 0.007$  with  $\Omega/\omega_{\text{orb}}=1.551$ , that is equal to 0.23 Myr, with the corresponding  $t_{\text{sync}}$  value for the  $60 M_{\odot}$  at  $Z=0.007$  with  $\Omega/\omega_{\text{orb}}=1.557$ , that is equal to 0.08. Note that the MS lifetime for the  $60 M_{\odot}$  is about 55% the MS lifetime of the  $30 M_{\odot}$ , while  $t_{\text{sync}}$  for the  $60 M_{\odot}$  is about one third the value of  $t_{\text{sync}}$  for the  $30 M_{\odot}$ , indicating that  $t_{\text{sync}}$  normalized to the MS-lifetime decreases when higher initial mass stars are considered.

##### 4.2.2. Surface and internal rotation rates

Time-averaged surface velocities for all the models as a function of the initial mass, metallicity and orbital period are shown in Fig. 8. The curves labeled by an S show the cases of single star models or models of stars belonging to wide binary systems. The curves labeled with a value of an orbital period correspond to close binary models. The most remarkable points to be noticed are the followings:

- For single stars, we clearly see the impact of stronger mass losses for higher metallicities and higher stellar masses. This makes the time-averaged surface velocities to decrease when the metallicity increases and when the initial mass increases.
- In case of close binary stellar models which are spin-down by tidal interactions (see the left panels), we see that at low metallicity, the spin-down is well effective. All the surface velocities in the close binary systems are smaller than the surface velocities of the single star models. It is quite different at higher metallicities. For instance at  $Z = 0.014$ , the surface velocities in the close binary systems are larger than the surface velocities of the single star models. This might appear strange, since at the beginning we have a situation of spin down. What does happen here is that the spin down does occurs only up to the point when synchronization is achieved. Once synchronization is reached, the transfer of angular momentum from the orbit to the star compensates for the losses of angular momentum by the star due to stellar winds. Thus we have actually from that point an acceleration process which sets in.
- We see that the time-averaged velocities in the close binary systems are slightly larger at the higher than at lower metallicities. This comes from the fact that stars at high metallicities are larger than at low metallicities, implying that for a given surface angular velocity, imposed by synchronization, the surface linear equatorial velocities are larger at high than at low metallicity<sup>2</sup>.
- Globally the cases of spin-up and spin-down are very similar. The largest differences occur for the  $60 M_{\odot}$  at  $Z = 0.014$  for a period equal to 1.4 days, the time-averaged surface velocity is equal to  $400 \text{ km s}^{-1}$  in the case of spin-down and to  $370 \text{ km s}^{-1}$  in case of spin-up. This comes from the fact that the synchronization is obtained more rapidly in the spin-down case than in the spin-up case because the initial rotation, in the spin down case is much nearer from the synchronized one than in the case of spin-down (see Table A.2).

All the models with tidal interactions show a very low degree of contrast between the central and the surface angular velocity.

##### 4.2.3. Evolutionary tracks

All the tracks for the primaries in various close binary systems are shown in Fig. 7. For all the initial masses, the close binary tracks will be comprised between the following two extreme cases: the single fastest rotating track at  $Z=0.002$  and the single slowest rotating track at  $Z=0.014$ . We see also that the close binary tracks show great similarities for the spin-down (upper panels for each mass) and the spin-up (lower panels for each mass), which is indeed expected (this is particularly visible in the case of the  $30 M_{\odot}$ ).

In the left panel of Fig. 9, we indicate the models that follow a homogeneous evolution. We used a very strict and conservative criteria for considering that a star follows a homogeneous evolution, namely, only those models evolving blueward along a straight line (until they enter into a WR phase) are considered to evolve homogeneously. There is no difference between the spin-down and spin-up cases. For each metallicity and initial mass, there exists an upper value for the orbital period below which stars evolve homogeneously. These upper limits are indicated in Table 1. We see that the conditions for having a homogeneous evolution in close binary systems are more restricted at low than

<sup>2</sup> the angular surface velocity is determined by synchronization and thus depends only on the orbital period, but not on the initial metallicity.

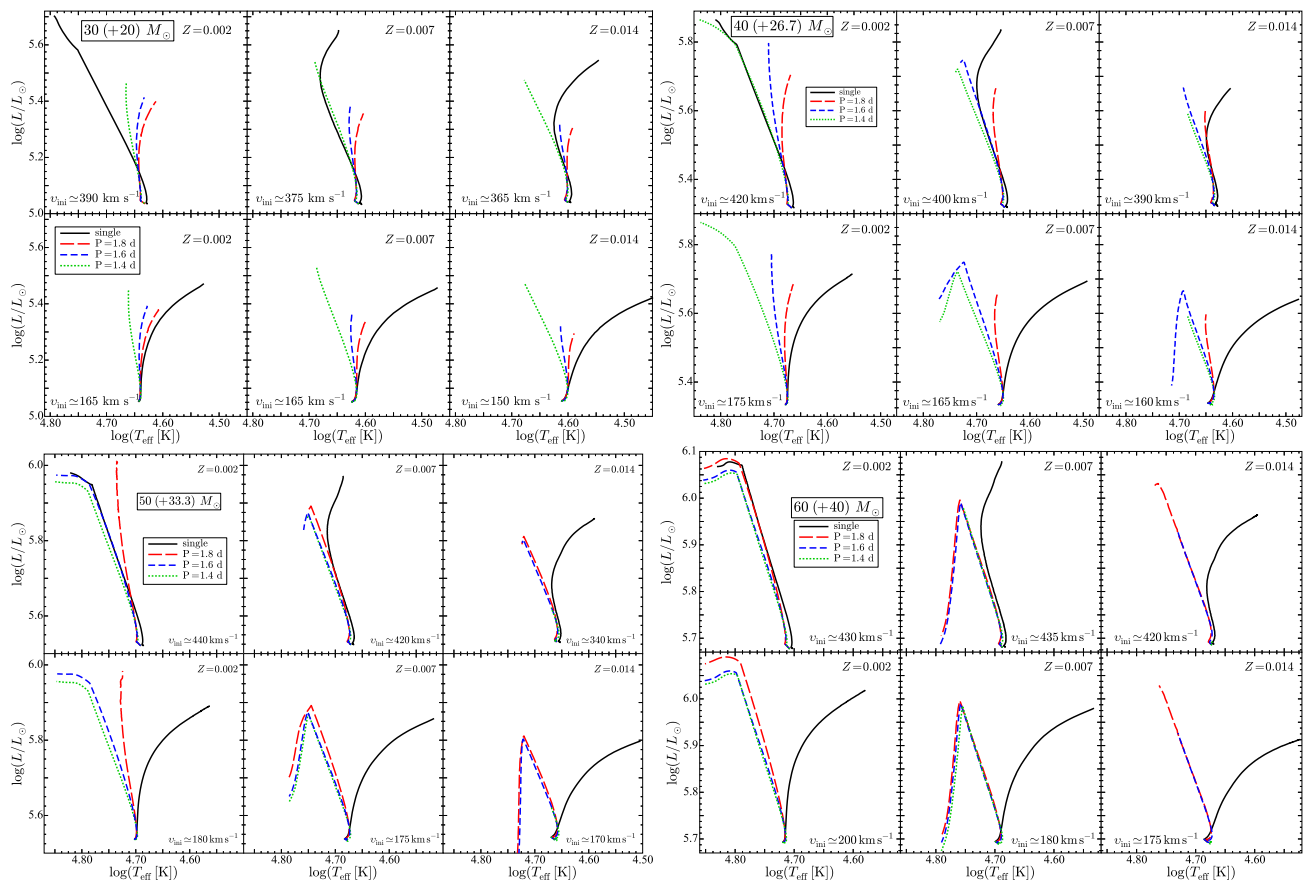


**Fig. 7.** Evolutionary tracks in the HR diagram for single star models and close binaries. The four panels correspond to different initial masses for the single star or for the primary in the close binary (in that case, the secondary has a mass equal to 2/3 the primary mass). The masses, the initial metallicities ( $Z$ ) and the approximate initial surface velocities on the ZAMS are indicated. For the precise initial surface rotation of each model look at the values in Tables A.1 and A.2. For a given initial mass, the three upper panels correspond to spin-down cases, while the three lower panels correspond to spin-up cases.

at high metallicities (the upper limits for the periods are smaller at  $Z=0.002$  than at  $Z=0.014$ ). We explain the reason for this in the next subsection.

All computations have been performed for a single value of the mass ratio between the secondary and the primary equal to 2/3. One can wonder how things change when this ratio varies. For a given mass of the primary and a given initial orbital period, a higher mass ratio implies stronger tides and thus a more rapid synchronization time. Note that keeping the period constant, assuming a more massive secondary star implies that the distance between the two components is larger, thus, a priori, it is not obvious that tides are stronger. This can however be seen using the third Kepler's law and equation (6) in paper I for the synchronization time. Thus a higher mass ratio favors homogeneous evolution through the decrease of the synchronization time<sup>3</sup>.

#### 4.2.4. Mixing and Roche lobe overflow during the MS phase

Let us begin by discussing the cases of the 30  $M_{\odot}$  models in Fig. 6. Looking at the single models (see right upper panels of Fig. 6), we recall the following main features: mixing is more important when the initial rotation is larger and the metallicity smaller. We see also that, at low metallicity, the fast rotating model enters the Wolf-Rayet phase at the end of the MS phase.

<sup>3</sup> Note that the angular velocity of the stars at synchronization is fixed by the orbital period and thus, provided this quantity is kept fixed, the mass ratio has no impact on the post-synchronization angular velocity.

**Table 1.** Maximum initial periods,  $P_{\max}$ , in days for having a homogeneous evolution for different initial mass stars (in solar masses) and metallicities and for a mass ratio of 3/2. When  $P_{\max}$  is larger than the largest period, respectively, smaller than the smallest period explored in this work, the symbols  $>$  and  $<$  are used.

Mass	$Z=0.002$	$Z=0.007$	$Z=0.014$
60	$> 1.8$	$> 1.8$	$> 1.8$
50	1.7	$> 1.8$	$> 1.8$
40	1.5	1.7	1.7
30	$< 1.4$	1.5	1.5

Now, when a companion is present with an orbital period comprised between 1.4 and 1.8 days, both in the spin-down and in the spin-up models, stars are more mixed (see for instance how the triangles are shifted to smaller values in binary models). We even see that the initially fast rotating model which is spin down (lower panel in the third column) enters the WR stage at the very end of the MS phase at  $Z=0.014$ , while the single corresponding model does not. As explained above this is due to the fact that, although this model is in a first phase spin-down, it will be actually spun up after synchronization in order to keep the surface spin angular velocity equal to the orbital angular velocity. This maintains a larger rotation than in the single star model which is continuously spun down by stellar winds. We see that

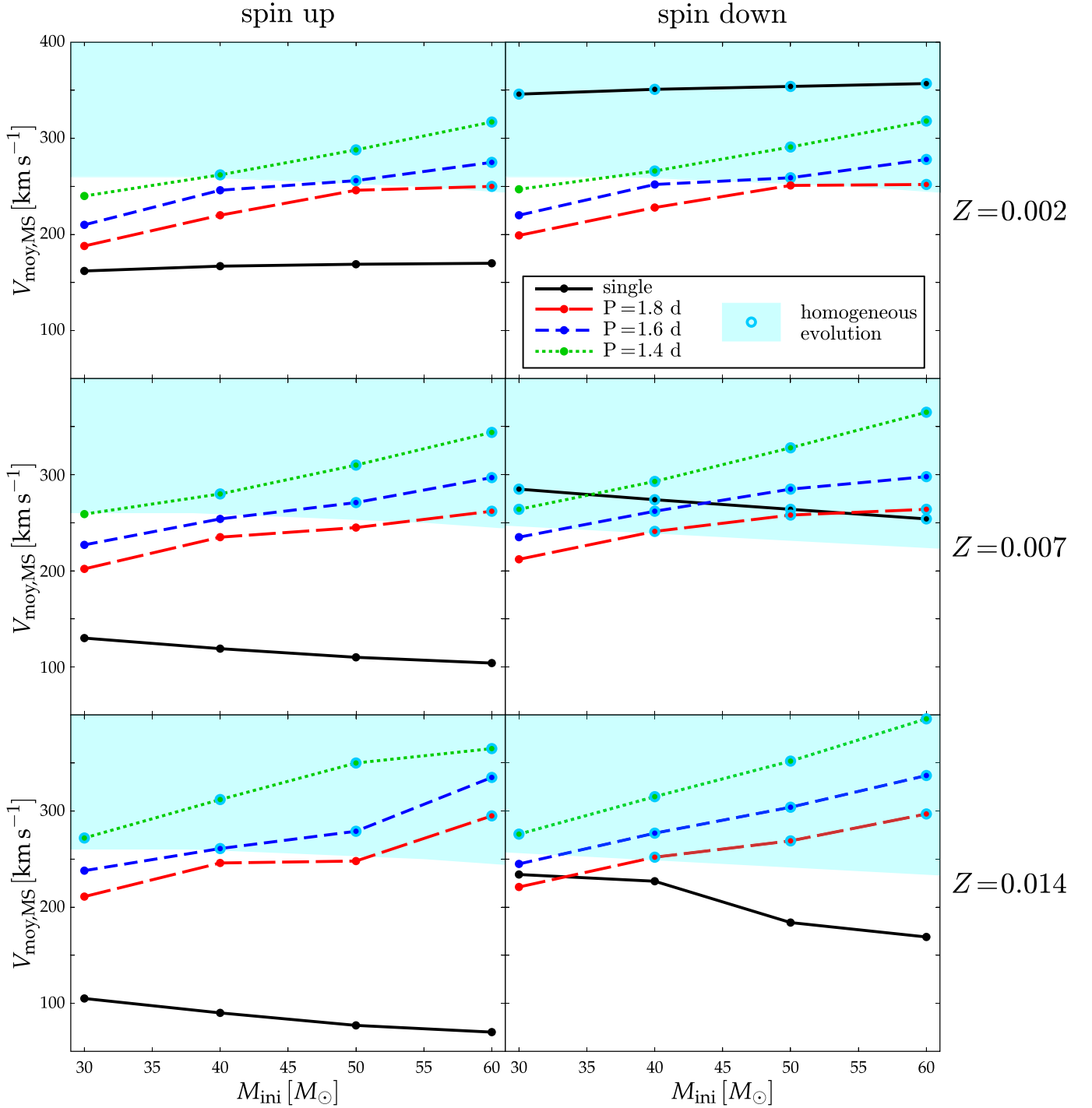


**Fig. 8.** Time-averaged surface equatorial velocity of single and binary stars as a function of the initial mass for various metallicities. The (black) continuous line connects the single star models. The (colored) dashed lines connect the binary stellar models. The initial period in days is indicated. The results corresponds to a companion having  $2/3$  the mass of the primary. The (blue) big dots show the models that follow a homogeneous evolution. The zone where homogeneous models lay in these diagram is hatched in blue. The panels on the left column correspond to spin-down cases and the panels on the right column to spin-up cases.

for all these models, Roche lobe overflow will occur before the end of the MS phase. Therefore for these models, we have never a situation where the Roche lobe overflow can be avoided during the MS phase.

Let us now discuss the case of the  $60 M_{\odot}$  models. The same qualitative features as for the  $30 M_{\odot}$  models can be seen for the plots representing the single star models. We just note that these more massive models are more mixed than the corresponding  $30$

$M_{\odot}$  models. For binary models, we note the following striking features:

- As in the case of the  $30 M_{\odot}$  model, stars with tidal interactions are more mixed, whatever they belong to a system where a spin-down or a spin-up occurs.
- One of the most striking point is the fact that mixing does appear to be more efficient in binary system at higher than at lower metallicity, in strong contrast with what happens

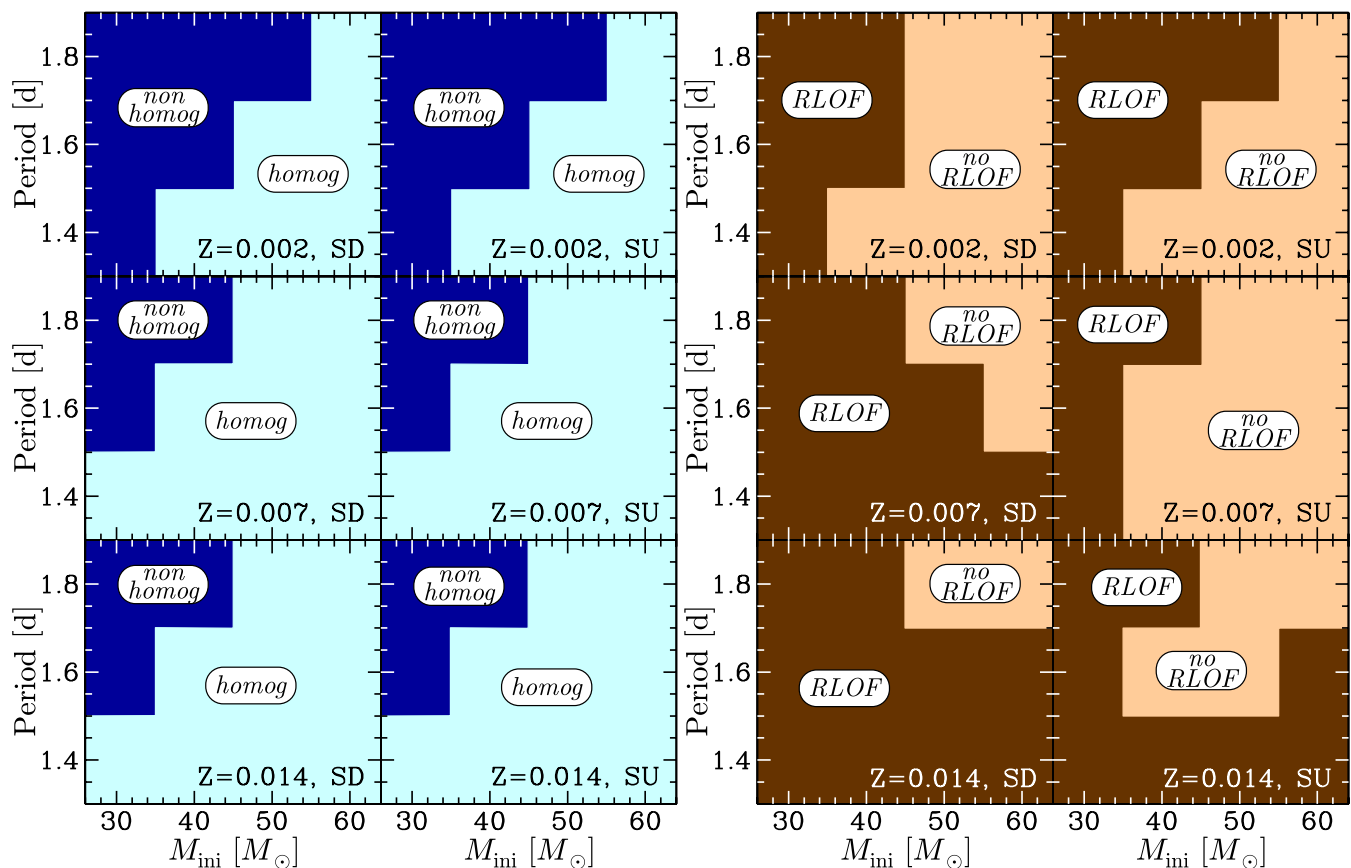


**Fig. 9.** The vertical axis is the initial orbital period in days, the horizontal axis is the initial mass of the primary in a close binary system. The secondary has a mass equal to  $2/3$  the mass of the primary. The different panels correspond to different initial metallicities  $Z$  and to different initial rotation of the primary. The letters SD are for Spin-Down cases. The letters SU are for Spin-Up cases. *Left panel:* A homogeneous evolution during the Main-Sequence phase occurs where *homog* is indicated (light blue areas). Non-homogeneous evolution during the Main-Sequence phase occurs where *non homog* is indicated (dark blue areas). *Right panel:* Roche lobe overflow during the Main-Sequence phase is avoided where *no RLOF* is indicated (light brown areas). Roche lobe overflow during the Main-Sequence phase occurs where *RLOF* is indicated (dark brown areas).

for single stars (look for instance to the panels for the  $60 M_{\odot}$  models for an orbital period equal to 1.8 days, This is less visible for the shorter periods because the models meet the Roche limit). We explain this change of behavior in the following way: in the present models, the driving effects for chemical mixing are the meridional currents. It is well known that the meridional velocity in the outer layers varies as the inverse of the density. Models which are at higher metallicity have larger radii and thus shallower outer envelopes, and hence larger meridional currents. This favors mixing at higher metallicity. For single stars however, mass loss by stellar winds may strongly reduce the angular momentum content and since meridional currents also scale with  $\Omega$ , mass losses may counteract the above effect, making the mixing less strong at higher metallicity. In close binary systems, the tidal locking may keep in the star an angular momentum larger than the one it would have if evolving without any tidal interaction. In that case,  $\Omega$  is kept constant and everything being equal (same mass), the model with a higher metallicity will be more strongly mixed. Such an effect will be more marked in high mass star models which have a shallower envelope than in small initial mass stars.

- Comparing the spin-up and the spin-down cases, we see that they are very similar given an orbital period. This is expected since the synchronization timescale is short in both cases (although see the remark below) and the velocities to which the

models converge are similar since imposed by the orbital period. A careful comparison between these two cases show however a slight asymmetry between the spin-down and the spin-up cases: the spin-up cases are in general more mixed than the spin-down ones. These differences are mostly due to the fact that spin-up models starts with initial angular velocities that are slightly nearer from the orbital period than the spin-down models (see Tables A.1 and A.2). Moreover, as explained in the Appendix B, in case of solid body rotation, the synchronization time is shorter in case of spin-up than in case of spin-down.

- All the  $60 M_{\odot}$  models at  $Z=0.002$  avoid a Roche lobe overflow during the MS phase (for the orbital periods considered here).

If we look at the panels for the two intermediate masses, 40 and  $50 M_{\odot}$ , we obtain qualitative similar behaviors. We can just note that, given an orbital period, higher the initial mass, stronger the effects of the tidal forces are (let us remind here that in all the cases the companion has a mass equal to  $2/3$  the mass of the primary).

In the right panel of Fig. 9, we indicate the models that show no Roche Lobe Overflow during the MS phase. We can note a few interesting points:

- Except in one case (the spin-down case for the  $50 M_{\odot}$  at  $Z=0.002$ ), every time a RLOF is avoided during the MS

phase, the star has a homogeneous evolution. On the other hand, not all models having a homogeneous evolution avoid a RLOF episode during the MS phase. Therefore the region of RLOF avoidance during the MS phase is in general smaller than the region of homogeneous evolution. This comes from the two opposite conditions for homogeneous evolution and RLOF avoidance: RLOF avoidance is more difficult when the initial periods are short, while homogeneous evolution is favored by short periods.

- RLOF avoidance is favored for higher masses (more mixed) and lower metallicity (more compact) models.
- Due to differences in the initial conditions for the spin-up and spin-down cases, as well as due to differences in the synchronization timescales we have different situations in case of spin-down and spin-up. For this feature, initial conditions have a significant impact. In general the spin-up cases more often avoids a RLOF episode during the MS phase.

We discussed above the impact on the efficiency of the mixing of changing the mass ratio, keeping the mass of the primary and the initial orbital period the same. We indicated that a higher mass ratio favors shorter synchronization time and thus stronger mixing. This effect favors RLOF avoidance. But one has also to account for the variation of the Roche limit with the mass ratio. For a given mass of the primary and a given initial orbital period, the Roche limit is larger in systems with larger mass ratios<sup>4</sup>. This implies that a higher mass ratio favors RLOF avoidance.

## 5. Consequences of tidal interactions

As explained in the previous section, tidal interactions in sufficiently close systems trigger strong mixing. In the present models, this strong mixing is induced by the high rotation imposed by the tidal coupling.

We may wonder whether these binary models have an evolution equivalent to a single star starting its evolution on the ZAMS with a rotation equal to the one obtained after synchronization in the close binary system? The answer is no especially at high metallicity. The main difference between these two cases is that the single star will lose a lot of angular momentum by stellar winds while the component in the close binary system will lose mass by stellar winds but not angular momentum, since the angular momentum lost by the winds will be replenished at the expense of the orbital angular momentum by the tidal interactions. Therefore in these systems, the close binary interaction is not only important to provide the star with a given initial rotation but also for maintaining this rotation all along the evolution until Roche lobe episode occurs.

The strong mixing may induce a homogeneous evolution and thus, as was already found by de Mink et al. (2009a), may make the primary to avoid Roche lobe overflow episode. From the present results, we can deduce the following conditions favoring such a scenario: first obviously the orbital period should not be too small. For a given binary system, indeed, smaller the orbital period, more difficult it will be to avoid Roche lobe overflow even when stars are strongly mixed. Second, conditions are more favorable in more massive systems, which are those in which mixing is the strongest. We see for instance that no one of the binary systems containing a  $30 M_{\odot}$  avoids Roche lobe overflow during the MS phase, whatever the metallicity considered, while

for instance many cases of the systems with a  $60 M_{\odot}$  models avoids such an overflow during the MS phase. Finally, we see that a lower metallicity constitutes also a favorable condition for avoiding Roche lobe overflow. Typically all the considered binary system with a  $60 M_{\odot}$  avoids Roche lobe overflow during the MS phase at  $Z=0.002$ , while at  $Z=0.014$ , only the case with an orbital period equal to 1.8 days avoids it. Note that this last point may be surprising in view of the conclusion reached in the previous section where it was indicated that models in close binary are more mixed at higher metallicities. We could have expected that if they are more mixed, they keep more compact and thus would more easily avoids the Roche lobe overflow. But things are not so simple indeed. Actually stars are more mixed at higher metallicities because they have a more extended envelope and a more extended envelope makes the reaching of the Roche limit more easy! At low metallicities, stars remain more compact and this favors the avoidance of the Roche lobe overflow.

We saw in the present work, that tidal interactions can provide to the primary in close binary systems sufficient angular momentum for triggering a homogeneous evolution. This implies that the radiative envelope is rich in CNO-processed material at early times along the MS phase. Some mass will be lost by the stellar winds and some mass can be lost at the moment of the mass transfer on the secondary in case the mass transfer is non-conservative. This material, lost by the system, if used to form new stars, will produce stars with some signature of CNO processing. This might be a possible channel to explain second generation stars in globular clusters.

Close binaries have already been invoked in this context by de Mink et al. (2009b). These authors propose that the secondary is accelerated to the critical velocity through mass accretion from the primary. When the critical limit is reached, the mass lost by the primary can no longer be accreted by the secondary and is therefore lost in the interstellar medium. At that point, the primary may have lost sufficient mass for layers having been processed at least partially by the CNO burning to be uncovered. This mass constitutes material that can be used to form new stars that would show surface abundances with signatures of CNO processing. So in that scenario, the CNO processed matter is extracted from the primary because previous mass losses have uncovered H-burning regions and the mass is lost because the secondary has reached the critical velocity. In the scenario we propose, CNO processed material is obtained very soon during the evolution due to the mixing triggered by tidal interactions. The mass at the moment of the mass transfer can be lost because of the same reason invoked by de Mink (the reaching of the critical limit by the secondary) or other effects. Typically, the secondary, if massive enough, loses some mass by stellar winds. This may prevent it to accrete part or all the material lost from the primary. We shall discuss the impact of such models in the frame of the origin of the anticorrelations in globular clusters in a forthcoming paper.

Could such an evolution be a plausible scenario for long soft Gamma Ray Bursts? At the moment, we cannot provide an answer to that question since it requires the computation of more advanced stages of the evolution of the systems. However, it is interesting that tidal interactions can trigger homogeneous evolution of the primary, makes it to enter the WR phase at an early stage in its evolution, while keeping a high angular momentum content. Of course the story is not finished and it may be that there will be still some mass transfer when the secondary would evolve in redder parts of the HRD. In cases however where no further mass transfer occurs or, if it occurs, that most of the mass would be lost by the system, then the present scenario

<sup>4</sup> This comes from the fact that to keep the same orbital period in systems with more massive components, the distance between the two components needs to be larger.

could be an interesting one for making fast rotating black holes from objects with no hydrogen-rich envelope. Interestingly, such a scenario might explain the existence of long soft gamma ray burst even at high metallicity. Single fast rotating models with strong internal coupling lose a lot of angular momentum by stellar winds at high metallicity making the conditions for obtaining simultaneously a fast rotating black hole from a progenitor having lost its H-rich envelope very difficult. Here, as we saw, tidal interactions can do two things that are favorable for obtaining these conditions, it produces mixing and, even when mass is lost, it replenishes the star in spin angular momentum.

How can the present models be tested by observations? Present models can be checked through the observations of the surface abundances of short period binary systems before any mass transfer has occurred. These systems will be most likely synchronized in view of the very short timescale for this process to occur. The determination of the orbital period will determine also the axial rotation of the two components. If some indications are obtained on the initial mass, metallicity of the system, then the observed surface abundances can be compared to the predictions of the present computations. Note that, whatever was the initial rotation of the primary, the surface abundances after synchronization will be the same. So the initial rotation of the components is not a critical parameter which is indeed a nice feature since this parameter cannot be estimated in a model independent way. Thus these close binary models represent very interesting targets to check rotational mixing (see also de Mink et al. 2009a).

Another prediction of the present models is that the primary of all close binary systems with an orbital period equal or inferior to 1.4 days, with a primary more massive than  $40 M_{\odot}$ , a companion having a mass equal to  $2/3$  of the primary, for metallicities  $Z$  equal or larger than 0.002 will follow a homogeneous evolution. Stars that follow a homogeneous evolution are over-luminous for their mass. All these models at  $Z = 0.002$  avoid a Roche Overflow event during the MS phase.

Close binary evolution may produce very fast rotating Wolf-Rayet (WR) stars as can be seen from Tables A.1 and A.2. Indeed, equatorial velocities between 160 and  $360 \text{ km s}^{-1}$  can be obtained through the binary channel. The corresponding single star models entering a WR phase have surface velocities at that stage between typically 20 and  $80 \text{ km s}^{-1}$ . Gräfener et al. (2012) deduced rotational properties inferred from photometric variability for six WR stars (see their table 3 and references therein). Three of them present surface velocities between 110 and  $230 \text{ km s}^{-1}$ . Such high surface velocities would be more in agreement with a close binary evolution.

## 6. Conclusions and perspectives

In this work, we studied the evolution of single and binary stellar models with a strong internal coupling.

For single stars, we showed that higher the initial mass, the initial rotation, lower the metallicity, stronger the mixing efficiency. This is exactly the same as in models with a moderate coupling, although the physics for the mixing between these two kinds of models is very different. In mildly coupled models, mixing is triggered by the gradients of  $\Omega$ , while in strongly coupled models, it is driven by  $\Omega$ . We obtain also that stars with a strong internal coupling, all other ingredients kept the same, are more strongly mixed than models with a moderate coupling.

When a companion is present, we checked that, as is well known, the synchronization time is very short. So that the main effect of the companion will be to lock the rotation around the

orbital rotation. The evolution after the synchronization process depends on the angular momentum at the synchronization time. The higher this angular momentum content is, the higher the degree of mixing. There is little dependence of the results on the initial velocity of the star. The angular momentum after synchronization is of course the highest in the systems with the shortest orbital periods.

Large differences between single and close binary models with initial masses above about  $30 M_{\odot}$  having similar initial rotation occur at large metallicities. The main difference comes from the fact that the single star model is spun down by losses of angular momentum by the stellar winds, while the angular momentum lost by the star in the close binary system is replenished by the tidal interactions. In that case, mass losses induce an acceleration of the star once synchronization is achieved.

We note also that, in contrast with the single star models, higher the metallicity, more efficient the mixing in the close binary models.

We have obtained some indications for the limiting orbital period below which our models will follow a homogeneous evolution. The conditions for homogeneous evolution are more restricted at low metallicity for the reason just mentioned above (less efficient mixing in low metallicity environments).

Quite generally, when no Roche Lobe Overflow occurs during the MS phases, the star has a homogeneous evolution. Not all models evolving homogeneously avoid a RLOF episode. RLOF avoidance is favored in high mass star models at low metallicity.

How can we check these models through observations? Ideally, one would like to observe close eclipsing binaries for which it is possible to obtain the masses of the components and from spectroscopy their position in the HR diagram as well as some indications of their surface abundances. These systems should be observed at a stage before any mass transfer. They would be likely synchronized since synchronization time is too short for allowing the observation of a system before it is synchronized.

From an analysis of these data, we could check the following points: first, we can see whether these stars present surface enrichments. We see that for short enough periods, surface enrichments are predicted for many models, with or without a magnetic field<sup>5</sup>. Second we can check whether stars are over-luminous for their initial mass, indicating that indeed they are strongly mixed. Third we can deduce their surface velocities. This last point is very important to discriminate between two classes of models: actually the present models with strong internal coupling predict strong mixing only for models with a high surface velocities (this is because the triggering of the mixing is  $\Omega$  and not the gradient of  $\Omega$ ). On the other hand, models with mild internal mixing mainly driven by shear can produce models which are strongly mixed and show a low surface velocity (Song et al. 2013). Note that these characteristics can also be obtained in single star evolution models when braking occurs by a magnetic coupling between the surface of the star and the stellar wind (Meynet et al. 2011).

<sup>5</sup> Note that stars following a homogeneous evolution show a carbon to hydrogen ratio at the surface that decreases in a first phase and then increases. This non-monotonic behavior comes from the fact that, in these nearly homogeneous models, both carbon and hydrogen vary in an important manner. Since the CN equilibrium is reached very rapidly, the first phase corresponds to the decrease of carbon while the abundance of hydrogen changes little. Thus the C/H ratio decreases. The second increasing part of the curve comes from the fact that carbon remains more or less constant (it has reached the CNO equilibrium value), while the abundance of hydrogen decreases. This makes this ratio to increase with time.



Finally let us mention that the present evolutionary scenario might be interesting to consider in the frame of the origin of the anticorrelation in globular clusters and for explaining the progenitors of some long soft Gamma Ray Bursts especially those which might appear in metal-rich regions. Close binary evolution seems to be needed to explain the existence of fast rotating Wolf-Rayet stars.

*Acknowledgements.* The authors thank the anonymous referee who helped through his very constructive remarks to improve this paper. This work was sponsored by the National Natural Science Foundation of China (Grant No. 11463002) and the Key Laboratory for the Structure and Evolution of Celestial Objects, Chinese Academy of Sciences (Grant No. OP201405). This work was supported by the Swiss National Science Foundation (project number 200020-146401).

## Appendix A: Some properties of the stellar models

Some properties of the single and binary models computed in this work are presented in Tables A.1 and A.2: The first four columns specify the model considered providing information about its status as a single or a component in a binary system with a given orbital period, the ratio of the initial surface angular velocity to the critical velocity on the ZAMS, the ratio of the initial surface angular velocity to the orbital one, as well as the initial equatorial rotation velocity. The five following columns indicate respectively the different times defined at the beginning of Section 4. The last three columns give some properties of the last computed model:  $X_c(\text{end})$  is the mass fraction of hydrogen at the center,  $v_{\text{eq}}(\text{end})$  is the surface equatorial velocity and  $N/C(\text{end})$  the ratio at the surface of the mass fractions of nitrogen to carbon normalized to the initial ratio. The initial ratio is the same for the three metallicities and is equal to 0.29 in mass fraction.

## Appendix B: Tidal interaction in close binary systems: impact of two different transport mechanisms for the angular momentum

In paper I (Song et al. 2013), we studied the effects of tidal interaction in close binary systems consisting of a 15 and a 10  $M_{\odot}$  star. We considered that the mechanisms for the transport of the angular momentum inside the star were the meridional currents and the shear instabilities. Here, we computed the models accounting for the Tayler-Spruit dynamo which is a much more efficient transport mechanism for the angular momentum and which imposes, at every time, a distribution of the angular velocity inside the star very close to a solid body rotation. In order to see how these different transport mechanisms affect various properties of the single and close binary stars, we compare the results obtained for 15  $M_{\odot}$  models computed with these two methods and starting with exactly the same initial conditions.

### Appendix B.1: Spin-down case

Let us begin discussing the spin-down case for a 15  $M_{\odot}$  model having a 10  $M_{\odot}$  companion with an initial orbital period of 1.4 days. In Fig. B.1, the evolution of the difference between the actual surface angular velocity  $\Omega$  and the orbital angular velocity  $\omega_{\text{orb}}$  for the cases without (continuous line) and with an internal magnetic field (dashed line) are shown. Note that the case without an internal magnetic field corresponds to a model already studied in paper I (Song et al. 2013). The left panel of the figure shows the evolution of the difference between the actual surface angular velocity and the orbital one normalized to the

orbital one. The right panel is a zoom on the very beginning of the slowing down process and show the difference between the actual velocity and the orbital one with no normalization.

We see that the evolution is quite similar in models with and without an internal magnetic field. This comes from the fact that at the beginning the two models present very similar characteristics (e.g. both are solid body rotating). Actually, we can see that both models enter the regime where they have a surface angular velocity differing from the orbital one by less than 20% very rapidly. This illustrates the well known fact that indeed synchronization is a very rapid process (see e.g. the discussion in de Mink et al. 2009a).

How the actual synchronization timescale obtained by the numerical models compares to the values obtained from analytic formulae? An interesting quantity is  $t_{\text{rot}}$  (see for instance Eq. 6 in Paper I);  $t_{\text{rot}}$  corresponds to the time that is needed to decrease the quantity  $\Omega - \omega_{\text{orb}}$  by a factor  $e$  (on the left panel of Fig. B.1 this corresponds to a decrease of one dex in the ordinate scale).

For evaluating  $t_{\text{rot}}$  from the analytical formula, we use the characteristics of the models on the ZAMS. The formula involve the moment of inertia of the region where the tidal force applies. Thus, this timescale will vary a lot depending on which portion of the star is considered to estimate the moment of inertia. In case the moment of inertia of the whole star is considered, the time is obviously longer than when only the moment of inertia of the outer layer is considered. Plugging the moment of inertia of the whole star in the analytic formula implicitly assumes that any change of the angular momentum at the surface has instantaneously an impact on the angular momentum in the core. This corresponds to the strongest coupling we can imagine and this implies the longest synchronization time (the tides have to slow down the whole star and not only its outer layers. When transport by magnetic fields are assumed, we have a situation approaching that of an instantaneous redistribution). The case of considering the moment of inertia of only the outer layers would correspond to the other extreme case where there is no coupling between the core or the region below these outer layers and these outer layers. In that case, synchronization is obtained more rapidly since a much smaller mass needs to be spun up or spun down. These examples show that numerical models with some moderate internal coupling will be in-between these two cases.

Is it the situation obtained here by the numerical models? Yes it is. To see that let us consider the specific case of the 15  $M_{\odot}$  model at  $Z=0.014$  in close binary system with a companion of 10  $M_{\odot}$  and with an orbital period of 1.4 days. The value for  $t_{\text{rot}}$  is equal to 38100 years plugging the moment of inertia of the whole star in the analytic formula (Eq. 6 in Paper I). This timescale corresponds to about 0.3% of the Main-Sequence lifetime of a non-rotating solar metallicity 15  $M_{\odot}$  model, whose Main-Sequence lifetime is about 11 My.

Let us now determine from the numerical model the time needed to decrease by a factor  $e$  the quantity  $\Omega - \omega_{\text{orb}}$ . The value of  $\omega_{\text{orb}}$  corresponding to a period of 1.4 days is equal to  $0.052 \text{ s}^{-1}$ . The horizontal dotted line on the right panel of Fig. B.1 shows the values  $(\Omega - \omega_{\text{orb}})/e$ . We see that the intersection between the curve showing  $\Omega - \omega_{\text{orb}}$  (continuous curve) and the dotted line occurs at a time  $t=0.174 \text{ Myr}$ . Now the start time of the model is not 0 but the time  $t_0 = 0.114 \text{ Myr}$  because the model needs some time to settle into a ZAMS structure. So the duration for decreasing  $\Omega - \omega_{\text{orb}}$  by a factor  $e$  is equal to  $174000 - 114000 = 60000 \text{ years}$ . Actually this is above the value deduced from the analytic formula by about a factor 2.

This might be at first sight surprising when considering that the analytic formula should already be an upper limit, but the an-

**Table A.1.** Some properties of the single and binary models for initial masses equal to  $30 M_{\odot}$  and  $40 M_{\odot}$ . In case the model is in a binary, the companion has an initial mass of respectively 20 and  $26.7 M_{\odot}$ . The symbol S is for single star models and the symbol BN.N is for close binaries with an orbital period equal to N.N days. For each metallicity and initial mass, eight models have been computed, four with a high initial rotation and four with a moderate initial rotation. When in binaries, the fast rotating cases correspond to tidally spin-down cases, while the moderately rotating ones correspond to spin-up cases. A small line in the column  $t_{\text{WR}}$  indicates that the star does not become a WR star before any RLOF or during the MS phase.

Model	$\frac{\Omega_{\text{ini}}}{\Omega_{\text{crit}}}$	$\frac{\Omega_{\text{ini}}}{\Omega_{\text{orb}}}$	$v_{\text{ini,eq}}$ km s <sup>-1</sup>	$t_{\text{sync}}$ 10 <sup>6</sup> yr	$t_{\text{N/C}}$ 10 <sup>6</sup> yr	$t_{\text{hom}}$ 10 <sup>6</sup> yr	$t_{\text{WR}}$ 10 <sup>6</sup> yr	$t(\text{end})$ 10 <sup>6</sup> yr	$X_{\text{c}}(\text{end})$	$v_{\text{eq}}(\text{end})$ km s <sup>-1</sup>	N/C(end)
<b>30 (+20) <math>M_{\odot}</math></b>											
<b>Z = 0.002</b>											
S	0.66	–	391	–	0.81	1.76	7.12	8.24	0.035	79	307
B1.4	0.66	1.772	394	0.34	0.45	1.35	–	6.17	0.24	292	272
B1.6	0.54	2.025	311	0.54	0.40	1.25	–	5.75	0.25	267	131
B1.8	0.66	2.279	394	0.81	0.38	1.21	–	5.64	0.22	242	90
S	0.30	–	163	–	2.54	1.08	–	6.38	0.041	142	17
B1.4	0.30	0.769	167	0.17	0.93	1.23	–	6.02	0.26	292	186
B1.6	0.30	0.879	164	0.17	1.22	1.12	–	5.54	0.26	267	69
B1.8	0.30	0.989	164	0.00	1.41	1.09	–	5.45	0.24	242	41
<b>Z = 0.007</b>											
S	0.66	–	374	–	0.83	1.75	–	8.02	0.035	58	369
B1.4	0.66	1.551	377	0.23	0.59	1.48	6.15	6.96	0.19	285	345
B1.6	0.66	1.773	377	0.36	0.60	1.32	–	5.59	0.30	270	131
B1.8	0.66	1.995	377	0.54	0.58	1.25	–	5.37	0.29	248	76
S	0.30	–	163	–	2.54	1.08	–	6.38	0.040	58	10
B1.4	0.30	0.769	167	0.17	0.93	1.23	–	6.88	0.20	286	341
B1.6	0.30	0.879	164	0.17	1.22	1.12	–	5.47	0.31	270	86
B1.8	0.30	0.989	164	0.00	1.41	1.09	–	5.18	0.30	249	41
<b>Z = 0.014</b>											
S	0.66	–	362	–	0.92	1.55	–	7.62	0.041	23	369
B1.4	0.66	1.411	365	0.18	0.64	1.53	6.20	6.73	0.24	281	345
B1.6	0.66	1.613	365	0.29	0.69	1.33	–	5.12	0.36	270	131
B1.8	0.66	1.815	365	0.43	0.71	1.25	–	4.86	0.35	250	76
S	0.30	–	151	–	3.44	1.01	–	6.24	0.056	31	9
B1.4	0.30	0.622	151	0.11	0.61	1.48	–	6.72	0.24	281	379
B1.6	0.30	0.711	151	0.38	0.97	1.22	–	5.03	0.37	270	93
B1.8	0.30	0.800	151	0.45	1.31	1.10	–	4.71	0.36	251	38
<b>40 (+26.7) <math>M_{\odot}</math></b>											
<b>Z = 0.002</b>											
S	0.66	–	416	–	0.51	1.88	5.28	6.24	0.035	57	286
B1.4	0.66	1.607	419	0.16	0.23	1.35	5.02	6.00	0.036	207	286
B1.6	0.66	1.837	419	0.24	0.20	1.12	–	5.37	0.15	302	362
B1.8	0.66	2.066	419	0.36	0.18	1.02	–	4.84	0.20	280	224
S	0.30	–	173	–	1.54	0.84	–	5.10	0.041	129	23
B1.4	0.30	0.704	174	0.07	0.33	1.25	5.0	5.98	0.040	205	286
B1.6	0.30	0.804	174	0.13	0.55	0.99	–	5.25	0.16	302	303
B1.8	0.30	0.905	174	0.00	0.70	0.90	–	4.70	0.22	280	114
<b>Z = 0.007</b>											
S	0.66	–	397	–	0.51	1.57	6.09	6.09	0.035	24	344
B1.4	0.66	1.401	401	0.08	0.30	5.03	4.89	5.03	0.25	272	344
B1.6	0.66	1.601	401	0.16	0.30	1.29	5.13	5.29	0.19	245	341
B1.8	0.66	1.802	401	0.24	0.27	1.10	–	4.69	0.25	277	248
S	0.30	–	166	–	1.71	0.80	–	5.10	0.040	29	19
B1.4	0.30	0.617	166	0.06	0.24	5.28	4.89	6.14	0.041	208	314
B1.6	0.30	0.705	166	0.10	0.39	1.20	5.14	6.02	0.041	190	314
B1.8	0.30	0.793	166	0.20	0.60	0.97	–	4.62	0.25	277	274
<b>Z = 0.014</b>											
S	0.69	–	401	–	0.55	1.31	–	5.21	0.18	33	310
B1.4	0.66	1.268	387	0.06	0.32	4.16	–	4.16	0.37	318	386
B1.6	0.66	1.450	387	0.13	0.34	1.40	4.92	4.92	0.26	278	369
B1.8	0.66	1.631	387	0.19	0.34	1.12	–	4.32	0.31	275	286
S	0.30	–	160	–	1.93	0.77	–	4.81	0.095	17	17
B1.4	0.30	0.540	161	0.05	0.20	4.16	–	4.16	0.37	318	386
B1.6	0.30	0.640	161	0.08	0.32	1.36	4.91	6.14	0.040	160	338
B1.8	0.30	0.720	161	0.24	0.50	1.03	–	4.29	0.31	275	248



**Table A.2.** Some properties of the single and binary models for initial masses equal to  $50 M_{\odot}$  and  $60 M_{\odot}$ . In case the model is in a binary, the companion has an initial mass of respectively 33.3 and  $40 M_{\odot}$ . Same comments as in the caption of Table 1.

Model	$\frac{\Omega_{\text{ini}}}{\Omega_{\text{crit}}}$	$\frac{\Omega_{\text{ini}}}{\Omega_{\text{orb}}}$	$v_{\text{ini,eq}}$ km s <sup>-1</sup>	$t_{\text{sync}}$ 10 <sup>6</sup> yr	$t_{N/C}$ 10 <sup>6</sup> yr	$t_{\text{hom}}$ 10 <sup>6</sup> yr	$t_{\text{WR}}$ 10 <sup>6</sup> yr	$t(\text{end})$ 10 <sup>6</sup> yr	$X_c(\text{end})$	$v_{\text{eq}}(\text{end})$ km s <sup>-1</sup>	N/C(end)
<u>50 (+33.3) <math>M_{\odot}</math></u>											
<u>Z = 0.002</u>											
S	0.66	–	436	–	0.35	2.14	4.32	5.19	0.035	46	286
B1.4	0.66	1.490	440	0.07	0.16	4.71	3.96	5.01	0.035	219	266
B1.6	0.66	1.702	440	0.12	0.14	1.25	4.10	4.98	0.036	191	266
B1.8	0.66	1.915	440	0.18	0.13	1.00	–	4.78	0.08	299	183
S	0.30	–	182	–	1.07	0.69	–	4.40	0.040	98.7	31
B1.4	0.30	0.654	183	0.05	0.17	4.71	–	4.98	0.040	222	266
B1.6	0.30	0.748	183	0.07	0.17	1.11	4.1	4.97	0.040	194	266
B1.8	0.30	0.841	183	0.10	0.39	0.88	–	4.62	0.12	307	286
<u>Z = 0.007</u>											
S	0.66	–	416	–	0.37	1.51	5.01	5.06	0.035	35	34
B1.4	0.66	1.294	420	0.04	0.19	4.05	3.97	4.05	0.27	306	345
B1.6	0.66	1.479	420	0.09	0.19	4.26	3.98	4.26	0.22	256	334
B1.8	0.66	1.664	420	0.12	0.19	1.23	4.13	4.23	0.22	248	334
S	0.30	–	174	–	1.17	0.67	–	4.37	0.041	19	31
B1.4	0.30	0.569	174	0.04	0.13	4.64	3.9	5.18	0.041	205	303
B1.6	0.30	0.650	174	0.05	0.19	4.50	3.98	5.12	0.041	178	307
B1.8	0.30	0.732	174	0.13	0.29	1.14	4.14	5.04	0.041	158	307
<u>Z = 0.014</u>											
S	0.66	–	403	–	0.39	1.15	–	4.84	0.035	14	331
B1.4	0.57	1.138	338	0.00	0.21	1.63	–	1.63	0.58	356	34
B1.6	0.57	1.301	338	0.04	0.23	3.97	3.94	3.97	0.27	291	355
B1.8	0.57	1.404	338	0.07	0.26	1.44	3.98	4.06	0.28	235	355
S	0.30	–	168	–	1.29	0.64	–	4.11	0.091	12	28
B1.4	0.30	0.517	169	0.04	0.11	1.63	–	1.63	0.57	356	383
B1.6	0.30	0.590	169	0.04	0.16	4.38	3.94	5.24	0.041	153	314
B1.8	0.30	0.664	169	0.10	0.24	1.41	3.98	5.14	0.041	134	334
<u>60 (+40) <math>M_{\odot}</math></u>											
<u>Z = 0.002</u>											
S	0.66	–	454	–	0.28	2.17	3.74	4.54	0.035	41	266
B1.4	0.67	1.401	460	0.04	0.14	4.24	3.41	4.40	0.035	234	266
B1.6	0.67	1.601	426	0.08	0.12	4.13	3.41	4.37	0.035	200	266
B1.8	0.67	1.801	394	0.11	0.11	1.20	3.57	4.36	0.036	176	266
S	0.30	–	190	–	0.80	0.61	–	3.90	0.058	78	38
B1.4	0.30	0.608	212	0.03	0.10	4.23	3.40	4.38	0.040	237	266
B1.6	0.30	0.696	224	0.05	0.15	4.12	3.41	4.36	0.040	203	266
B1.8	0.30	0.783	190	0.08	0.23	1.04	3.62	4.34	0.040	180	266
<u>Z = 0.007</u>											
S	0.66	–	432	–	0.29	1.49	4.34	4.43	0.035	32	326
B1.4	0.66	1.211	437	0.03	0.13	3.38	–	3.38	0.30	365	335
B1.6	0.66	1.384	437	0.06	0.14	4.10	3.42	4.56	0.035	181	305
B1.8	0.66	1.557	437	0.08	0.14	3.96	3.43	4.51	0.036	158	305
S	0.30	–	181	–	0.86	0.60	–	3.89	0.048	16	13
B1.4	0.30	0.534	181	0.03	0.08	4.23	3.42	4.59	0.040	211	89
B1.6	0.30	0.611	181	0.04	0.11	4.09	3.41	4.53	0.041	183	88
B1.8	0.30	0.687	181	0.06	0.16	3.95	3.42	4.49	0.041	161	91
<u>Z = 0.014</u>											
S	0.66	–	418	–	0.30	1.05	–	4.26	0.035	12	27
B1.4	0.67	1.085	420	0.00	0.13	0.16	–	0.16	0.70	388	4.4
B1.6	0.69	1.240	440	0.04	0.15	3.54	3.39	3.54	0.26	330	351
B1.8	0.69	1.395	408	0.06	0.16	4.15	3.39	4.45	0.035	255	296
S	0.30	–	175	–	0.93	0.57	–	3.62	0.10	10	13
B1.4	0.30	0.483	175	0.03	0.07	0.17	–	0.17	0.70	382	4.1
B1.6	0.30	0.552	175	0.03	0.09	3.54	3.35	3.64	0.26	330	5.3
B1.8	0.30	0.620	175	0.05	0.13	4.17	3.39	4.43	0.041	292	86

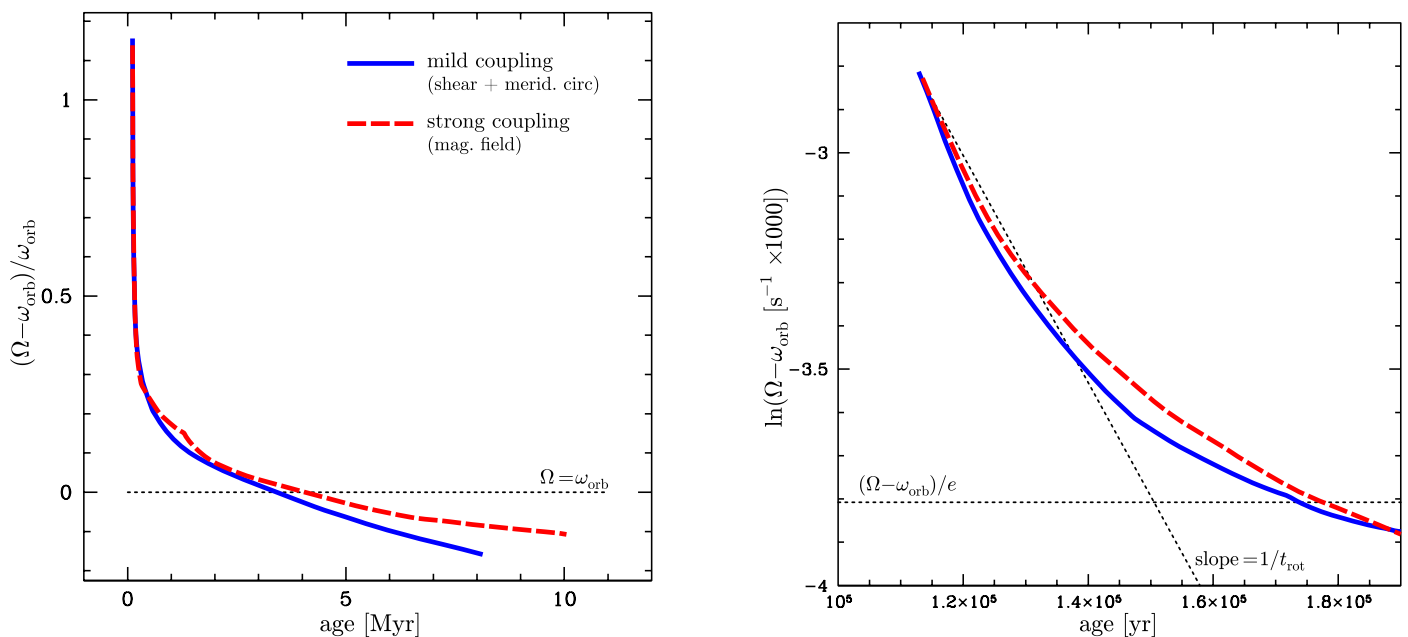


**Fig. B.1.** *Left panel:* Evolution as a function of time of the surface angular velocity,  $\Omega$ , minus the orbital angular velocity,  $\omega_{\text{orb}}$ , normalized to the orbital angular velocity for a  $15 M_{\odot}$  model at  $Z=0.014$  beginning its evolution on the ZAMS with an initial rotation around  $420 \text{ km s}^{-1}$  and an orbital period equal to 1.4 days. Its companion has  $10 M_{\odot}$ . The continuous (blue) line corresponds to models computed with a mild coupling mediated by shear and meridional currents. The dashed (red) line corresponds to models with a strong coupling mediated by an internal magnetic field (solid body rotation). The horizontal dotted line has an ordinate equal to 0, *i.e.* its intersection with the other curves indicates when an equality between  $\Omega$  and  $\omega_{\text{orb}}$  is obtained. *Right panel:* Evolution as a function of time of  $\Omega - \omega_{\text{orb}}$  (natural logarithm) for the same models as in the left panel. The horizontal dotted line is at an ordinate equal to  $(\Omega - \omega_{\text{orb}})/e$ . The other dotted line has a slope equal to  $1/t_{\text{rot}}$  as given by Eq. (6) in Paper I.

alytic formula is strictly valid only on a timescale during which  $\Omega - \omega_{\text{orb}}$  is not varying too much. Actually, as can be seen from Fig. B.1,  $\Omega - \omega_{\text{orb}}$  decreases very fast (actually  $\Omega$  is varying very fast since  $\omega_{\text{orb}}$  keeps a constant value) and thus  $t_{\text{rot}}$  is varying very fast too. Since  $\Omega$  tends towards  $\omega_{\text{orb}}$ ,  $t_{\text{rot}}$  increases, so that the actual time to decrease by a factor  $e$  can actually be larger than the value obtained from ZAMS properties. The increase is however modest. Indeed, 60000 years remains a very short value compared to the MS lifetime (less than 1%).

On the right panel of Fig. B.1, the slope at the beginning should be near the value given by  $1/t_{\text{rot}}$ . Interestingly, we can see that the slope at the ZAMS of the continuous line (model with shear and meridional currents without magnetic field) is steeper than the slope of the dotted line, indicating that indeed at the beginning, the synchronization time of the numerical model is shorter than the one obtained by the analytic formula, as expected. We see also that the model with an internal magnetic field (dashed line) has an intermediate position between the continuous and the dotted line also exactly as expected. This short discussion therefore demonstrates that the present results are indeed quite consistent.

We can note that the time when  $\Omega$  is equal to  $\omega_{\text{orb}}$  is around 3.5 Myr and 4 Myr for the non-magnetic and magnetic models respectively (see the intersections of the horizontal dotted line with the curves on the left panel of Fig. B.1). However from an observational point of view, the star can be said synchronized much earlier when typically the difference between these two angular velocities is less than 10-20%. Indeed, uncertainties pertaining the measures of the rotation velocity and of the stellar radius (to obtain  $\Omega$  from  $v_{\text{rot}}$ ) will make extremely difficult to identify the point when  $\Omega$  is equal to  $\omega_{\text{orb}}$ . Moreover, as can be seen from Fig. B.1, the decrease of  $\Omega$  is very rapid and important at the beginning making the star to be quasi-synchronized

in a very short time interval. We note also that after the point when  $\Omega = \omega_{\text{orb}}$ ,  $\Omega$  becomes slightly inferior to  $\omega_{\text{orb}}$ . This comes from the fact that the surface velocity of the star is governed by various processes with different timescales: the tidal forces which have a relatively long timescale when  $\Omega$  is near  $\omega_{\text{orb}}$ , the inflation of the envelope (nuclear timescale), the mass loss (the process becomes more important when evolution proceeds and has a rapid timescale), the internal transport mechanisms (which are rapid in that case). The global effect of all these processes on the surface angular velocity results from their interplay. It is natural that when  $\Omega$  is near  $\omega_{\text{orb}}$ , the tidal forces likely do no longer dominate, at least until the differences between those two quantities are not too large, and thus  $\Omega$  is maintained near  $\omega_{\text{orb}}$  but not exactly at a value equal to  $\omega_{\text{orb}}$ .

In Fig. B.2, the evolutionary tracks for the single  $15 M_{\odot}$  at  $Z=0.014$ , with an initial rotation on the ZAMS equal to  $\sim 420 \text{ km s}^{-1}$  is shown, together with the tracks of models with the same characteristics but now having a nearby  $10 M_{\odot}$  companion (orbital period equal to 1.4 days). One case is the same as the one presented in paper I and the other is computed with the Tayler-Spruit dynamo.

When no magnetic field is accounted for, as in paper I, we see that the model in the close binary system is more rapidly mixed than the single star model, hence the small shift to the left with respect to the single star model. The additional mixing in the binary model is due to the tidally induced shear mixing as explained in Song et al. (2013).

When the Tayler-Spruit dynamo is accounted for we see that the single star model is more mixed than the corresponding non-magnetic single star model. We see even that the mixing in that case is so efficient that the star follows the characteristic track of a nearly homogeneous star. This is in line with the results obtained by Maeder & Meynet (2005), who indeed noted that mod-

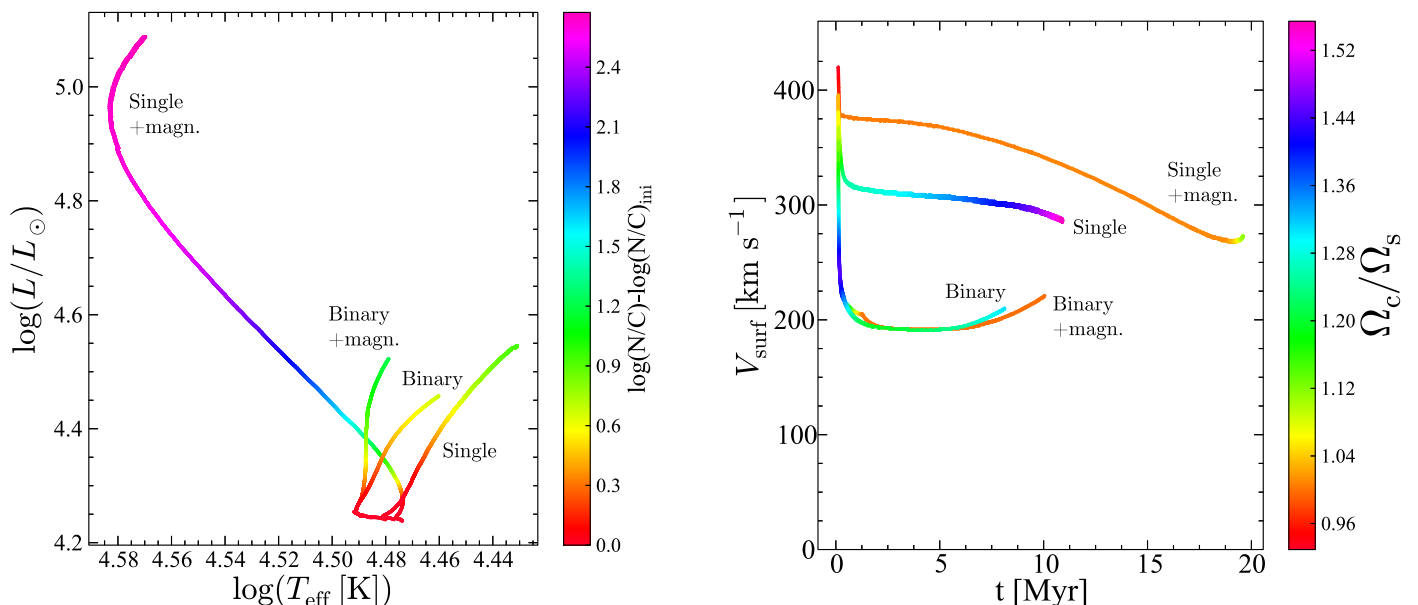


**Fig. B.2.** *Left panel:* Evolutionary tracks in the HR diagram for  $15 M_{\odot}$  at  $Z=0.014$  beginning their evolution on the ZAMS with initial rotation around  $420 \text{ km s}^{-1}$ . The track labeled *Single* is for an isolate star computed as in Paper I (transport of angular momentum by shear and meridional currents), the one labels with *Binary* is for a binary with an initial orbital period of 1.4 days computed with the same transport mechanisms as in Paper I. The models labeled *Single+magn.* and *Binary+magn.* are for single and binary stars respectively with similar characteristics but computed with the Tayler-Spruit dynamo. The color scale on the right shows the evolution of abundance ratio  $N/C$  at the surface normalized to the initial value on the ZAMS. *Right panel:* Evolution of the surface equatorial velocity for the same models as in the left panel. The color scale on the right shows the evolution of the ratio  $\Omega_c/\Omega_s$ .

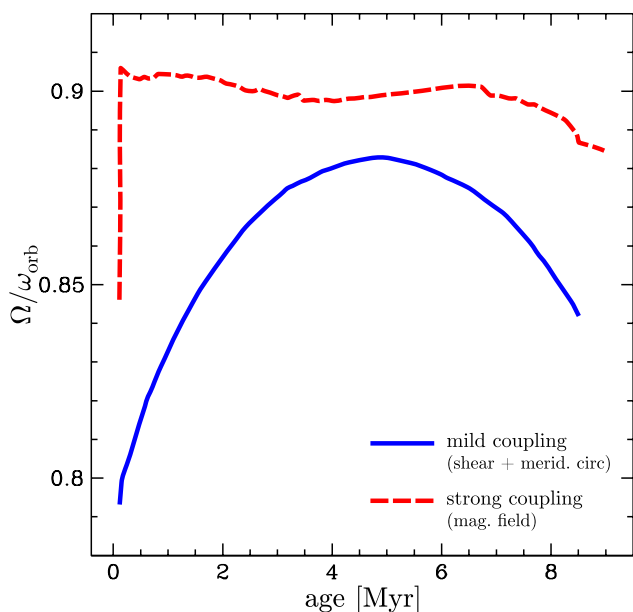


**Fig. B.3.** Evolution as a function of time of the ratio of the surface angular velocity to the orbital velocity for a  $15 M_{\odot}$  model at  $Z=0.014$  with an initial rotation of  $135 \text{ km s}^{-1}$  and with an orbital period of 1.4 days. The continuous lower curve corresponds to a model without magnetic field and the dashed upper curve corresponds to a model with an internal magnetic field.

els with magnetic fields were more strongly mixed than models without magnetic field, all other ingredients being kept the same. In this model, and this will also be true in the case of the binary model that we have discussed in the present paper, the mixing of the chemical elements is mainly governed by  $D_{\text{eff}}$ , which itself depend on  $U$  and thus on  $\Omega$ . This means that in these models,

the value of  $\Omega$ , and not that of the gradient of  $\Omega$  (as in models of Song et al. 2013), governs the transport of the chemical elements.

The binary model computed with the Tayler-Spruit dynamo is spined down by the synchronization process. Since  $\Omega$  is lower than in the single star model, the stellar model is less mixed. *Thus we see that a tidally induced spin-down triggers a more efficient mixing than in a single star in case the angular momentum is transported by shear and meridional currents and a less efficient mixing than in a single star when the angular momentum transport imposes a solid body rotation*<sup>6</sup>.

This is correct for the present  $15 M_{\odot}$  model which has weak stellar winds. When stellar winds are strong, then we saw in the present paper that a spin-down can trigger more mixing provided the angular momentum after synchronization is high enough. Actually, as we have explained in Section 3, the spin-down in these systems is rapidly replaced by a spin-up process triggered by strong mass losses.

An interesting consequence of this fact is that these models with strong coupling will never be able to explain those stars observed to be non-evolved, highly enriched and slowly rotating stars (see group 2 stars discussed in Hunter et al. 2009). Models with milder coupling as those studied in paper I or with a wind-magnetic braking mechanism (Meynet et al. 2011), in contrast, can produce stars showing these characteristics.

We note that the binary model with magnetic field is more mixed than the binary non-magnetic model. This is expected since the magnetic models are more mixed.

On the right panel of Fig. B.2, the evolution of the surface velocity is shown together with some indications on the internal gradient of angular velocity. The two single star models correspond to the upper lines. The magnetic coupling maintains a higher surface velocity than the coupling due only to shear and

<sup>6</sup> Whatever is the physical cause imposing this solid body rotation.

meridional currents. The single star model with an internal magnetic field has a very small contrast between the angular velocity at the center and the angular velocity at the surface. In case of the close binary systems, the surface velocities rapidly converge in the two cases toward more or less the same values as a result of the tidal forces. The magnetic model, as in the single star case, show very weak contrasts between the rotation of the core and that of the envelope.

### Appendix B.2: Spin-up case

Let us now compare the cases with and without magnetic field in case of spin-up. In Fig. B.3, the evolution as a function of time of the ratio of the surface angular velocity to the orbital velocity is shown for the magnetic and the non-magnetic model. We see that the magnetic model stabilizes very rapidly around a value equal to 90% the orbital velocity. The non-magnetic model takes more time to reach the maximum value equal to 88% the orbital period before to evolve away from it.

Why does the surface angular velocity of the star never reach the orbital one? As noted above, the evolution of the surface angular velocity results from many effects: tidal forces tend to make  $\Omega$  equal to  $\omega_{\text{orb}}$ , accelerating the star. On the other hand, the inflation of the radius, the transport of angular momentum inwards due to meridional currents and the loss of angular momentum by stellar winds slow down the surface. The evolution shown in Fig. B.3 result from all these processes. The fact that the surface angular velocity of the star only approaches the orbital one indicates that the acceleration coming from the tidal interactions cannot compensate in these models for the counteracting effects of the other processes, thus the synchronization can only be achieved up to a certain point. We note however that observation could hardly detect very precisely this kind of situation since when the surface angular velocity is already equal to 85-90% of the orbital one, it will be difficult to say that it is not equal to the orbital velocity in view of the uncertainties pertaining the measures of the surface rotations of stars and of their radii (in order to obtain the surface angular velocity). The decrease of  $\Omega$  towards the end of the computation results in part from larger mass loss rates and from more rapid inflation of the star.

In Fig. B.3, we can see also that the acceleration of the surface is more rapid in the magnetic than in the non-magnetic model. For the spin-down case, we just saw above, that the synchronization timescale increases when the coupling is stronger. Here we have the inverse situation. Why? In models with no magnetic field, we have that the meridional currents transport angular momentum from the surface to the core, hiding thus important amount of angular momentum deposited at the surface in the central region. This tends to slow down the synchronization process. In solid body rotating models, the core cannot rotate faster than the envelope, preventing the angular momentum to accumulate in the core. In that case, synchronization is more rapid. *Thus we see that in case of spin-down, a strong coupling makes the synchronization time longer than in cases of milder coupling, while in case of spin-up, a strong coupling makes the synchronization time shorter.*

The evolutionary tracks in the HRD for the 15  $M_{\odot}$  stellar models at  $Z=0.014$  with an initial rotation rate around 135  $\text{km s}^{-1}$  are very similar for isolate stars with or without an internal magnetic field. The same is true for the tracks of these same models in a close binary system with a 10  $M_{\odot}$  companion and having an initial orbital period of 1.4 days. This is why we do not show these tracks in a figure. The tracks do not differ much

because these systems keep relatively low velocities even in the case of spin-up by tidal forces. These models follow classical evolution and not a homogeneous evolution.

On the other hands, the models present at a given age very different values at the surface for the N/C ratio and the equatorial velocity as can be seen in Fig. B.4. We see that magnetic models are more mixed than non-magnetic ones (whatever single or in a binary system), that binary models are more mixed than single ones (whatever magnetic or not) and that the magnetic binary model is more mixed than the non-magnetic binary model. This last point is in contrast with the case of spin-down where the magnetic binary model was less mixed than the non-magnetic binary model. How can we explain this difference? As seen above, the spin-up timescale in the magnetic model is shorter than in the non magnetic one, thus the magnetic models reach earlier a level of higher rotation and thus has a higher mixing efficiency.

### References

- Brott, I., de Mink, S. E., Cantiello, M., et al. 2011, A&A, 530, A115  
 de Mink, S. E., Cantiello, M., Langer, N., et al. 2009a, A&A, 497, 243  
 de Mink, S. E., Pols, O. R., Langer, N., & Izzard, R. G. 2009b, A&A, 507, L1  
 Ekström, S., Georgy, C., Eggenberger, P., et al. 2012, A&A, 537, A146  
 Georgy, C., Ekström, S., Eggenberger, P., et al. 2013a, A&A, 558, A103  
 Georgy, C., Ekström, S., Granada, A., et al. 2013b, A&A, 553, A24  
 Gräfener, G., Vink, J. S., Harries, T. J., & Langer, N. 2012, A&A, 547, A83  
 Gratton, R., Sneden, C., & Carretta, E. 2004, ARA&A, 42, 385  
 Gratton, R. G., Carretta, E., & Bragaglia, A. 2012, A&A Rev., 20, 50  
 Groh, J. H., Meynet, G., Ekström, S., & Georgy, C. 2014, A&A, 564, A30  
 Hunter, I., Brott, I., Langer, N., et al. 2009, A&A, 496, 841  
 Leitherer, C., Ekström, S., Meynet, G., et al. 2014, ApJS, 212, 14  
 Levesque, E. M., Leitherer, C., Ekstrom, S., Meynet, G., & Schaerer, D. 2012, ApJ, 751, 67  
 Maeder, A. 1980, A&A, 92, 101  
 Maeder, A. 1987, A&A, 178, 159  
 Maeder, A. 2009, Physics, Formation and Evolution of Rotating Stars  
 Maeder, A. & Meynet, G. 2001, A&A, 373, 555  
 Maeder, A. & Meynet, G. 2005, A&A, 440, 1041  
 Martini, F., Depagne, E., Russeil, D., & Mahy, L. 2013, A&A, 554, A23  
 Martins, F., Hillier, D. J., Bouret, J. C., et al. 2009, A&A, 495, 257  
 Meynet, G., Eggenberger, P., & Maeder, A. 2011, A&A, 525, L11  
 Meynet, G., Ekström, S., Maeder, A., et al. 2008, in IAU Symposium, Vol. 250, IAU Symposium, ed. F. Bresolin, P. A. Crowther, & J. Puls, 147–160  
 Mowlavi, N., Meynet, G., Maeder, A., Schaerer, D., & Charbonnel, C. 1998, A&A, 335, 573  
 Sana, H., de Koter, A., de Mink, S. E., et al. 2013, A&A, 550, A107  
 Sana, H., de Mink, S. E., de Koter, A., et al. 2012, Science, 337, 444  
 Song, H. F., Maeder, A., Meynet, G., et al. 2013, A&A, 556, A100  
 Spruit, H. C. 2002, A&A, 381, 923  
 Yoon, S.-C., Langer, N., & Norman, C. 2006, A&A, 460, 199  
 Yusof, N., Hirschi, R., Meynet, G., et al. 2013, MNRAS, 433, 1114  
 Zahn, J.-P., Brun, A. S., & Mathis, S. 2007, A&A, 474, 145

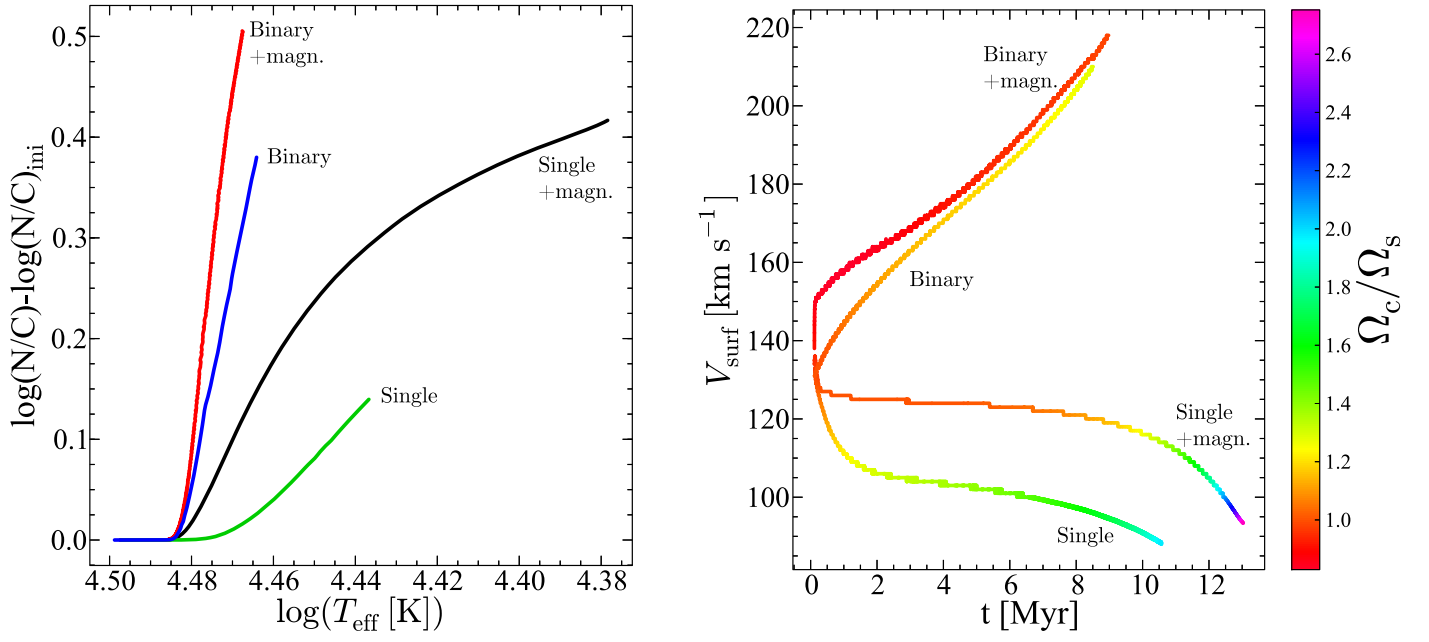


**Fig. B.4.** *Left panel:* Evolution of the abundance ratio  $N/C$  at the surface of  $15 M_{\odot}$  models at  $Z=0.014$  with an initial equatorial velocity of  $\sim 135 \text{ km s}^{-1}$  as a function of  $\lg T_{\text{eff}}$ . Binary models correspond to  $15 M_{\odot}$  with the same characteristics as indicated above but with a  $10 M_{\odot}$  companion and an initial orbital period of 1.4 days. *Right panel:* Evolution of the surface equatorial velocity as a function of time for the same models as in the left panel. The colors indicate the ratio between the central angular velocity and the surface one.